Upper plate faults may contribute to the paleoseismic subsidence record along the central Hikurangi subduction zone, Aotearoa New Zealand

Jaime Elizabeth Delano[1], Andrew Howell[2], Kate Clark[3], and Timothy Stahl[1]

[1]Univeristy of Canterbury
[2]University of Canterbury
[3]GNS Science

July 20, 2023

Abstract

Earthquake-driven subsidence can cause cascading hazards at the coast by exacerbating relative sea level rise, storm surges, tsunami, and tidal flooding. At Ahuriri Lagoon near Napier, Aotearoa New Zealand, paleoseismic uplift and subsidence is typically attributed to upper plate faults and subduction interface earthquakes, respectively. We test this assumption with elastic dislocation models of upper plate and subduction interface earthquakes informed by historical events, seismic surveys, and modern interface coupling data. We compared our surface deformation results to paleoseismic records preserved at Ahuriri Lagoon, which includes eight rapid subsidence (c. 0.5 to 1.2 m) and two rapid uplift events over the last c. 7 ky. Our models demonstrate that offshore upper plate faults could cause subsidence of c. 0.5 to 1 m at Ahuriri Lagoon at recurrence intervals of c. 2 kyr. A range of subduction interface earthquakes can also produce subsidence at Ahuriri Lagoon, and may explain larger (>1 m) subsidence, but must rupture the currently creeping (i.e., aseismic) portions of the interface. We demonstrate that both upper plate fault and subduction interface earthquakes may have contributed to the Ahuriri Lagoon records, and that interface coupling may be more heterogeneous than modern geodetic data suggest. Models of sea-level rise and earthquake multi-hazards that do not include the effects of upper plate faulting may mischaracterize risk at the coast.

Hosted file

964070_0_art_file_11018127_rv4wxj.docx available at https://authorea.com/users/541535/articles/645389-upper-plate-faults-may-contribute-to-the-paleoseismic-subsidence-record-along-the-central-hikurangi-subduction-zone-aotearoa-new-zealand

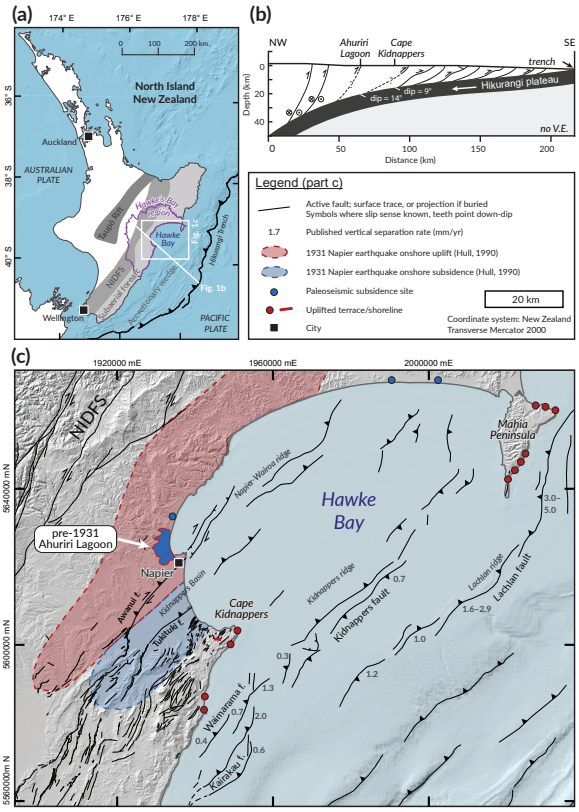
(a)
174° E
176° E
178° E
0
100
200 km
36° S
38° S
40° S
North Island
New Zealand
Auckland
AUSTRALIAN PLATE
Hikurangi Plateau
Ruatoria
Hikurangi Trough
Hawke Bay
Fig. 1b
NIDFS
Subducted ridge
Intermediate wedge
Wellington
PACIFIC PLATE
(b)
NW
SE
Ahuriri Lagoon
Cape Kidnappers
trench
Hikurangi plateau
dip = 14°
dip = 9°
no V.E.
Depth (km)
Distance (km)
Legend (part c)
Active fault; surface trace, or projection if buried
Symbols where slip sense known, teeth point down-dip
1.7
Published vertical separation rate (mm/yr)
1931 Napier earthquake onshore uplift (Hull, 1990)
1931 Napier earthquake onshore subsidence (Hull, 1990)
Paleoseismic subsidence site
Uplifted terrace/shoreline
City
20 km
Coordinate system: New Zealand
Transverse Mercator 2000
(c)
1920000 mE
1960000 mE
2000000 mE
5940000 mN
5900000 mN
5860000m N
NIDFS
Napier–Wairoa ridge
Hawke Bay
Mahia Peninsula
3.0–5.0
pre-1931 Ahuriri Lagoon
Napier
Cape Kidnappers
Kidnappers ridge
Kidnappers fault
0.7
1.0
Lachlan ridge
Lachlan fault
1.6–2.9
Kidnappers Basin
Awanui f.
Tukituki f.
0.3
1.2
1.3
Waimarama f.
0.7
2.0
0.4
0.6
Kairakau f.

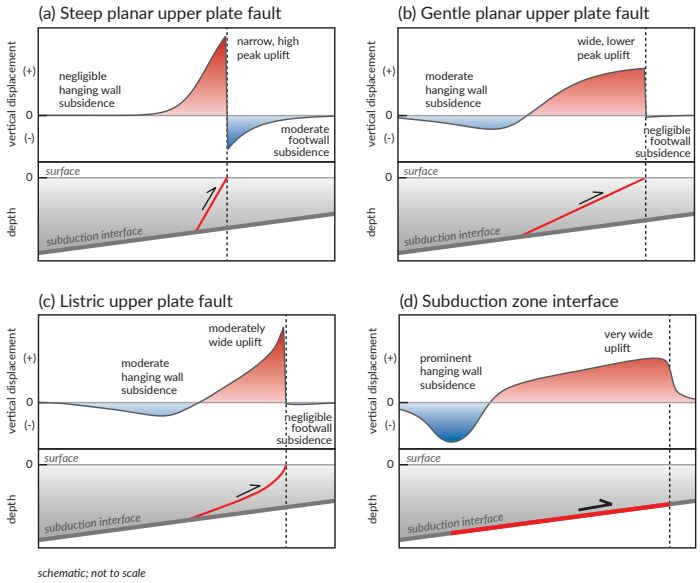

schematic; not to scale

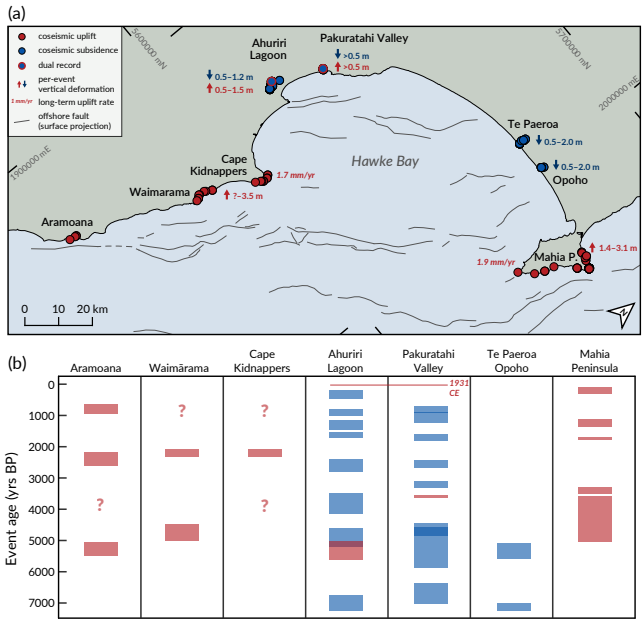
(a)
coseismic uplift
coseismic subsidence
dual record
per-event vertical deformation
1 mm/yr
long-term uplift rate
offshore fault (surface projection)
5600000 mN
5700000 mN
1900000 mE
2000000 mE
Ahuriri Lagoon
0.5–1.2 m
0.5–1.5 m
Pakuratahi Valley
>0.5 m
>0.5 m
Te Paeroa
0.5–2.0 m
0.5–2.0 m
Opoho
Hawke Bay
Cape Kidnappers
1.7 mm/yr
Waimarama
7–3.5 m
Aramoana
Mahia P
1.4–3.1 m
1.9 mm/yr
0 10 20 km
(b)
Aramoana
Waimārama
Cape Kidnappers
Ahuriri Lagoon
Pakuratahi Valley
Te Paeroa Opoho
Mahia Peninsula
1931 CE
Event age (yrs BP)
0
1000
2000
3000
4000
5000
6000
7000

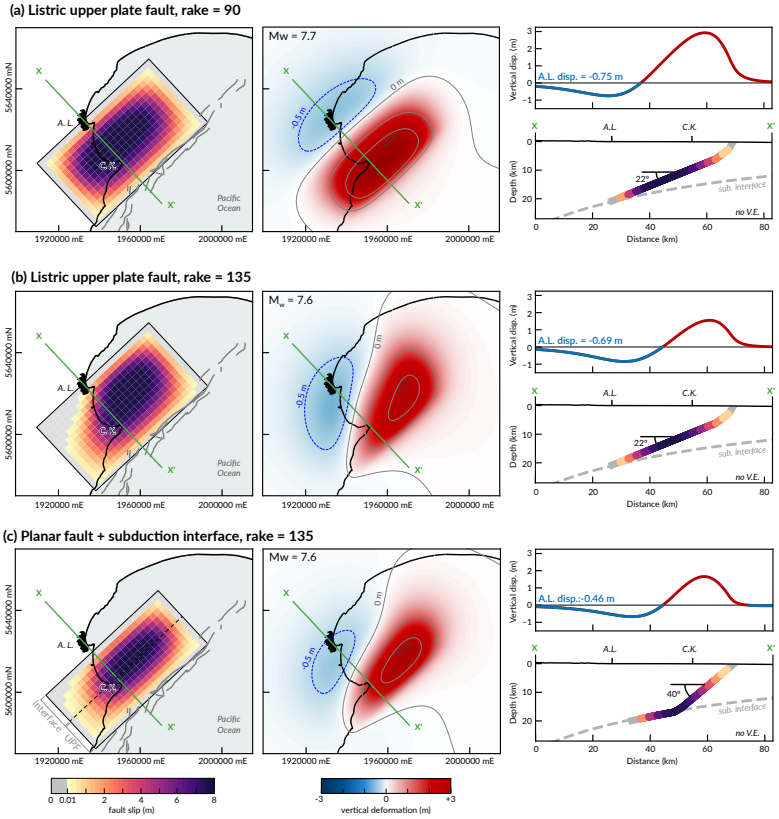
(a) Listric upper plate fault, rake = 90
Mw = 7.7
A.L. disp. = -0.75 m
(b) Listric upper plate fault, rake = 135
M_w = 7.6
A.L. disp. = -0.69 m
(c) Planar fault + subduction interface, rake = 135
Mw = 7.6
A.L. disp.=-0.46 m
A.L.
C.K.
Pacific Ocean
Sub. interface
no V.E.
Distance (km)
Depth (km)
Vertical disp. (m)
fault slip (m)
vertical deformation (m)

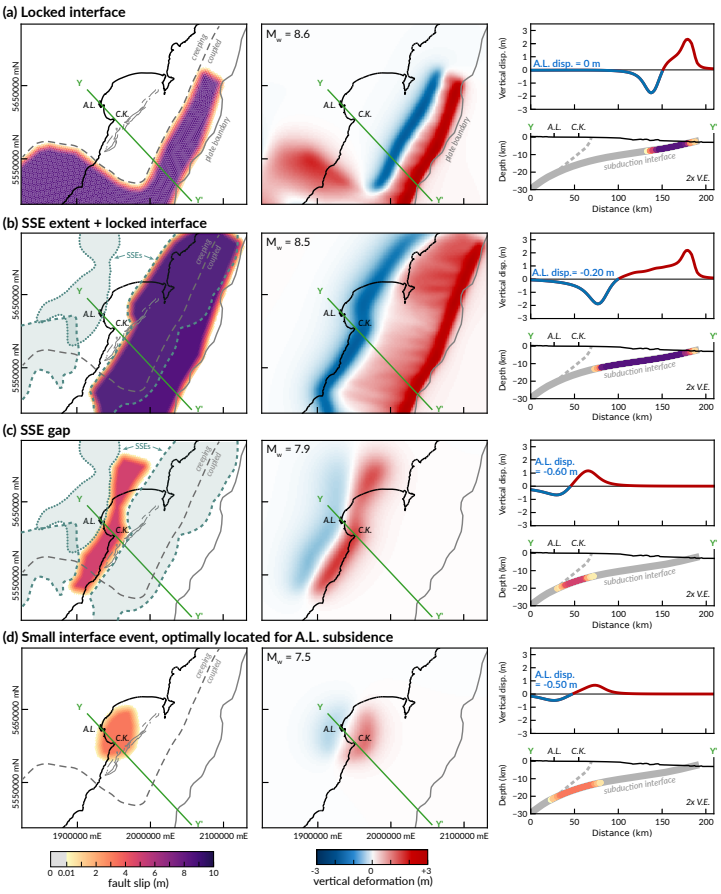

Hosted file

964070_0_supp_11018120_rv4wt1.docx available at https://authorea.com/users/541535/articles/645389-upper-plate-faults-may-contribute-to-the-paleoseismic-subsidence-record-along-the-central-hikurangi-subduction-zone-aotearoa-new-zealand

Upper plate faults may contribute to the paleoseismic subsidence record along the central Hikurangi subduction zone, Aotearoa New Zealand

J. E. Delano[1], A. Howell[1,2], K. J. Clark[2], and T. A. Stahl[1]

[1] School of Earth and Environment, Te Whare Wānanga o Waitaha | University of Canterbury, Christchurch, Aotearoa New Zealand.

[2] Te Pū Ao | GNS Science, Lower Hutt, Aotearoa New Zealand.

Corresponding author: Jaime Delano (jaimedelano@gmail.com)

Key Points:

- Elastic dislocation modeling shows listric upper plate faults can cause coastal coseismic subsidence above the down-dip rupture limit
- Coseismic subsidence at a key site (Ahuriri Lagoon, central Hikurangi margin) can be caused by both upper-plate and subduction earthquakes
- Subduction seismic cycle interpretations using coseismic uplift and subsidence records should consider the influence of upper plate faults

Abstract

Earthquake-driven subsidence can cause cascading hazards at the coast by exacerbating relative sea level rise, storm surges, tsunami, and tidal flooding. At Ahuriri Lagoon near Napier, Aotearoa New Zealand, paleoseismic uplift and subsidence is typically attributed to upper plate faults and subduction interface earthquakes, respectively. We test this assumption with elastic dislocation models of upper plate and subduction interface earthquakes informed by historical events, seismic surveys, and modern interface coupling data. We compared our surface deformation results to paleoseismic records preserved at Ahuriri Lagoon, which includes eight rapid subsidence (c. 0.5 to 1.2 m) and two rapid uplift events over the last c. 7 ky. Our models demonstrate that offshore upper plate faults could cause subsidence of c. 0.5 to 1 m at Ahuriri Lagoon at recurrence intervals of c. 2 kyr. A range of subduction interface earthquakes can also produce subsidence at Ahuriri Lagoon, and may explain larger (>1 m) subsidence, but must rupture the currently creeping (i.e., aseismic) portions of the interface. We demonstrate that both upper plate fault and subduction interface earthquakes may have contributed to the Ahuriri Lagoon records, and that interface coupling may be more heterogeneous than modern geodetic data suggest. Models of sea-level rise and earthquake multi-hazards that do not include the effects of upper plate faulting may mischaracterize risk at the coast.

Plain Language Summary

Earthquakes can cause land to uplift or subside. If land subsides along the coastline it becomes more susceptible to flooding, storm waves, tsunami, and ongoing seal level rise. The geologic record at Ahuriri Lagoon near Napier, New Zealand shows that earthquake have caused subsidence of at least 0.5 m many times over the last 7,000 years. We modeled how earthquakes on different faults, such as the subduction zone or smaller crustal faults above it, would vertically move the coastline. We found that both types of earthquakes have likely caused subsidence at Ahuriri Lagoon, which differs from past interpretations that focus mainly on subduction zone earthquakes. Additionally, the subduction earthquakes that cause subsidence at Ahuriri Lagoon are not in the expected location based on modern instrumental data. Therefore, future hazard models may need to take into account a broader range of earthquake source faults and more complex earthquake scenarios.

1 Introduction

Vertical deformation from earthquakes near the coast can cause meter-scale, near-instantaneous changes in relative sea level. In particular, coseismic subsidence can cause localized relative sea level rise (e.g., Kaiser et al., 2012) and worsen the effects of climate-driven sea level rise (e.g., Ministry for the Environment, 2022), tsunamis (e.g., Dura et al., 2021), storm surges (e.g., Muis et al., 2016), erosion (e.g., Bruun, 1962; Peterson et al., 2000), saltwater intrusion (e.g., Bosserelle et al., 2022), and tidal and groundwater flooding (Bosserelle et al., 2022; Sweet & Park, 2014). Geologic records of vertical deformation are critical for understanding fault behavior and models of the subduction zone seismic cycle (e.g., Atwater & Hemphill-Hayley, 1997; Berryman et al., 2018; Cochran et al., 2006; Philibosian and Meltzner, 2020; Sieh et al., 2008). Along subduction margins, both upper plate faults and the subduction interface may cause coseismic uplift and subsidence but the implications for hazard vary greatly between different fault sources (Clark et al., 2015). Understanding the source, character, and

likelihood of earthquake-driven coastal deformation is therefore important for hazard mitigation and forecasting how seismic and coastal hazards will impact communities.

The paleoseismic record at Ahuriri Lagoon (Hayward et al., 2016), situated above the Hikurangi subduction zone in Aotearoa New Zealand (Fig. 1), encapsulates many of the challenges involved in using pre-instrumental vertical coastal motions to constrain subduction behavior and associated seismic hazard. Numerous upper-plate faults are present in onshore and offshore Hawke's Bay (Fig. 1) and contribute to vertical motions at Ahuriri Lagoon. The M_w 7.8 1931 Napier earthquake ruptured the steep reverse-oblique Awanui fault and uplifted Ahuriri Lagoon by 1-2 m (Fig. 1) (Haines and Darby, 1987; Hull, 1990). The c. 7 kyr paleoseismic record there includes sudden subsidence (0.5-1.2 m per event) in eight inferred paleoearthquakes, as well as uplift in a further two events (including 1931 CE) (e.g., Hayward et al., 2016; Hull 1990).

Attributing specific fault sources to events at Ahuriri Lagoon and other sites along the Hikurangi margin is made difficult by wide age uncertainties, short record lengths, limited spatial preservation, and intertwined signals from subduction and upper plate fault earthquakes (e.g., Clark et al. 2019). Slip on upper-plate structures clearly controls the topography and sedimentary basin structure of the area over 10 kyr to 100 kyr timescales (e.g., Barnes et al., 2002; Berryman et al., 2011; Hull, 1987; Litchfield et al., 2022; Paquet et al., 2009). Despite this established role of upper-plate faulting in the structural evolution of the region, previous work has not identified upper-plate earthquake sources that explain coseismic subsidence at the lagoon. Consequently, paleoseismic subsidence at Ahuriri Lagoon has been tentatively attributed to subduction earthquakes, which are responsible for significant long-wavelength coseismic subsidence along other subduction margins (e.g., Atwater, 1987; Melbourne et al., 1997; Plafker, 1969; Subarya et al., 2006).

There have been no large subduction earthquakes along the Hikurangi margin in historical times that could guide expected patterns of coastal deformation. At many subduction zones, the spatial pattern of coupled or partially coupled segments corresponds to slip patches in past great earthquakes (e.g., Chlieh et al., 2008; Loveless & Meade, 2011; Perfettini et al., 2010) and therefore persistent coupling may inform future earthquake behavior (e.g., Chlieh et al., 2011; Kaneko et al., 2010; Lay & Nishenko, 2022; Uchida and Bürgmann, 2021; Wang, L., et al., 2015). Geodetic suggest predominantly low modern coupling on central Hikurangi subduction zone, meaning convergence is currently accommodated through slow-slip and aseismic (Wallace et al., 2004; Woods, 2022). The current understanding of strain accumulation and release generally suggests creeping portions of subduction zones are not expected to host large megathrust earthquakes (e.g., Wang, K., et al., 2012). Is modern Hikurangi interface behavior and coupling long-lived, and if so, which fault sources produced the coseismic subsidence observed at Ahuriri Lagoon?

The scarcity of subduction zone paleoseismic records along the Hikurangi margin highlights the importance of the relatively long record at Ahuriri Lagoon (Clark et al., 2019). The discrepancy between the inferred earthquakes in the Ahuriri Lagoon record and the modern low coupling along the central margin is difficult to reconcile. The current New Zealand National Seismic Hazard model takes a conservative approach to this problem and incorporates a higher coupling coefficient for the central Hikurangi interface than the geodetically derived values (Van Dissen et al., 2022; Wallace et al., 2020). Therefore, the Ahuriri Lagoon paleoseismic record currently underpins models that ultimately inform building codes, and improvements to fault source characterizations will have a direct impact on future mitigation.

In this study, we use elastic dislocation modelling to address two questions: (1) can recognized upper plate faults produce coseismic subsidence at Ahuriri Lagoon, and (2) what is the range of plausible subduction earthquakes that can cause subsidence at Ahuriri Lagoon? These slip models can explore a greater suite of potential earthquakes and resulting coastal deformation from upper plate faults and the subduction interface better than the spatially limited, short, and fragmentary paleoseismic records. This approach also allows for variations based on uncertainties in fault source geometries, kinematics, and slip which have never before been applied to the Ahuriri Lagoon paleoseismic records and are rarely considered elsewhere. Our results challenge the current paradigm that sudden coastal subsidence at Ahuriri Lagoon only records megathrust earthquakes, which merits reconsideration of the role of upper plate faults in the paleoseismic record and characterizing coastal earthquake hazards.

2 Background

2.1 Expected vertical deformation from upper plate fault and subduction earthquakes

Coastal coseismic deformation above the Hikurangi subduction zone is likely dictated by a complex interaction between slip along the subduction interface as well as from multiple smaller upper plate faults (Fig. 1). Both interface and upper plate fault earthquakes can produce uplift and subsidence (Fig. 2). Coseismic vertical deformation at the coast, such as at Ahuriri Lagoon, depends on the site location in relation to the source fault and rupture patch as well as fault dip. Steeper reverse faults produce significant hanging wall uplift and little-to-no hanging wall subsidence and may cause subsidence in the near-fault footwall; a similar signal occurred during the 1931 Napier earthquake (Fig. 1, Fig. 2a) (e.g., Haines & Darby, 1987; Hull, 1990). Gently dipping reverse faults (upper plate fault or interface) produce uplift above the up-dip portion of the rupture patch and subsidence above the down-dip limit of the rupture patch (Fig. 2b–2d) (e.g., Meltzner et al., 2006), or along strike from the slip patch (Briggs et al., 2014). Listric (curved) faults can produce large uplift near the fault tip and are capable of hanging wall subsidence due to steep dips at shallow depths and gentle dips at deeper depths (Fig. 2c) (e.g., Cochran et al., 2006).

These expected deformation patterns are the basis for many studies where coastal deformation records inform past earthquake behavior (e.g., Atwater & Hemphill-Haley, 1997; Clark et al., 2015; Cochran et al., 2006; Hayward et al., 2016; Witter et al., 2022) and longer-term subduction zone behavior (Meltzner et al., 2010, 2012; Sieh et al., 2008; Tsang et al., 2015; Woods, 2022). The dual uplift and subsidence record at Ahuriri Lagoon suggests at least two source faults contribute to coseismic deformation there (e.g., Hull, 1990). Attributing fault source and other interpretations from paleoseismic site data typically include assumptions about the source fault and slip behavior, but become less clear if multiple fault sources can produce similar coastal deformation signals at any one site (e.g., McNeill et al., 1998). In order to build realistic elastic dislocation models, we summarize below the known seismogenic fault sources in central Hawke's Bay and evidence that informs expected earthquake behavior at Ahuriri Lagoon.

2.2 Hikurangi subduction zone behavior

Large-magnitude subduction earthquakes have not been observed on the Hikurangi margin since European colonization in 1840 CE. Therefore, much of subduction zone earthquake characterization, expected slip behavior, and hazard forecasts are heavily informed by interface

coupling models (e.g., Van Dissen et al., 2022). Coupling estimates use modern geodetic motions to infer the degree of interface locking across the plate margin (e.g., Johnson et al., 2022; Wallace et al., 2004). Megathrust earthquakes are thought to occur in highly coupled (locked) zones, while aseismic processes, like slow slip and creep, are inferred to dominate in zones of low coupling (e.g., Herman & Furlong, 2021; Witter et al., 2014). The central Hikurangi margin has low coupling and has experienced multiple slow slip events in recent decades (Wallace et al., 2004, 2009). Some locking may occur near the trench, but geodetic data there, and thus coupling models, are poorly constrained (Wallace et al., 2004, 2009; Woods, 2022). Other studies that use vertical derivatives of horizontal strain suggest more heterogeneous coupling near Hawke's Bay with smaller locked patches between slow-slip event extents (Dimitrova et al., 2016). The relatively rough central Hikurangi interface, caused by subducted sea mounts and a change in interface protolith, likely contributes to the creeping and slow slip behavior and lack of large magnitude earthquakes (e.g., Wang, K., & Bilek, 2014)

The paleoseismic record along the central margin shows evidence of both large vertical displacements and tsunami deposits, indicative of larger magnitude stick-slip earthquake behavior, which is seemingly at odds with modern low coupling and slow-slip behavior (Clark et al., 2019; Hayward et al., 2016; Wallace et al., 2009). Whether the interpreted contemporary coupling reflects long-term subduction behavior, and whether the central margin will host great subduction earthquakes, remains unknown (Clark et al., 2019).

2.3 Coastal uplift records

The M_w 7.8 1931 Napier earthquake (also referred to as the 1931 Hawke's Bay earthquake; see McGinty et al. (2001)) is the only earthquake since 1840 CE that deformed the Hawke's Bay coast and likely occurred on the Awanui fault (Fig. 1c) (Hull et al., 1990; Kelsey et al., 1998). The earthquake produced a >90-km-long uplifted dome with peak uplift of 2.5 m, c. 1.5 m uplift at Ahuriri Lagoon, and up to 1.1 m of localized onshore subsidence in the proximal fault footwall (Fig. 1c) (Hull, 1990). Two additional paleoseismic uplift events are recorded in the combined Ahuriri Lagoon and Pakuratahi Valley sediments since 7 ka (Fig. 3) (Hayward et al., 2016; Pizer et al., 2022). These uplift events are attributed to the Awanui fault or similar faults in that zone.

Uplifted marine terraces farther east provide longer-term, time-averaged uplift records as well as individual paleoearthquake uplift data (Fig. 3). Mahia Peninsula uplift is considered dominantly controlled by the northwest-dipping Lachlan fault (discussed further below), and provides general constraints for a fast-slipping and well-characterized offshore structure (Fig. 1c) (Berryman, 1993a; Berryman et al., 2018; Clark et al., 2019). Uplifted terraces there record a minimum of five earthquakes since c. 4,500 yrs BP, per-event uplift of 1.4–3.1 m, and longer-term uplift rates up to 1.9 ± 0.5 mm/yr since 40 ka (Fig. 3) (Berryman, 1993b, 1993a; Berryman et al., 2018).

Farther south, uplifted Holocene marine terraces are preserved at Cape Kidnappers, Waimārama, and Aramoana and are attributed to earthquakes on the northwest-dipping Kidnappers Ridge, Waimārama, and Kairākau fault network (Fig. 1c) (Hull, 1987; Litchfield et al., 2022; Miyauchi et al., 1989; Paquet et al., 2011). These sites record one to three paleoearthquakes since c. 5.5 ka. The large height difference between some Holocene terraces indicate additional intermediate terraces, and thus records of past earthquakes, may have eroded away (Fig. 3) (Clark et al., 2019; Hull, 1987; Litchfield et al., 2022; Miyauchi et al., 1989). Pleistocene strandlines in central Cape Kidnappers provide an uplift rate of 1.6 mm/yr since c.

120 ka (Hull, 1985; Paquet et al., 2011). Other less well-preserved Pleistocene strandlines at the eastern Cape Kidnappers margin have been used to infer an uplift gradient across Cape Kidnappers, however, both strandlines are undated (Fig. S1). We use only the central, better-preserved strandline for constraints in this study.

2.4 Coastal subsidence records

Localized footwall subsidence in the 1931 Napier earthquake is the only historical coseismic subsidence in central Hawke's Bay (Fig. 1c). Longer records of coseismic subsidence in Hawke's Bay are inferred from lagoon sediments that record repeated rapid relative sea level rise events. The best-studied and most complete records are from Ahuriri Lagoon, which shows eight subsidence events ranging from 0.5–1.2 m over the last c. 7 ka (Fig. 3) (Hayward et al., 2015, 2016; Hull, 1986). These geologic records provide evidence for abrupt subsidence events (i.e., from earthquakes) rather than from post- or interseismic processes. Hayward et al. (2016) also found an additional 1.6–2 m of subsidence since 7 ka at Ahuriri Lagoon that could not be confidently attributed to earthquakes.

Initial studies of coseismic subsidence at Ahuriri Lagoon did not interpret possible source faults for these events, but recognized a potential link to the overall fold structure between Napier and Cape Kidnappers (Hull, 1986). The 1931 Napier earthquake source fault, other upper plate faults, and the seismogenic potential of the subduction zone were not understood at the time. More recent studies inferred that some, if not all, subsidence events were caused by subduction interface earthquakes because similar phenomena occurred along other margins (Hayward et al., 2006, 2016).

Some Ahuriri Lagoon subsidence events correlate with paleoseismic events elsewhere along the Hikurangi margin (≥70 km along-margin distance), suggesting widespread deformation and strong ground motions, and thus a larger (i.e., subduction interface) fault source (Clark et al., 2019; Hayward et al., 2016; Pizer et al., 2022). The adjacent Pakuratahi Valley and more northerly Te Paeroa/Opoho sites also record multiple rapid subsidence and tsunami deposits in the Holocene, some of which have overlapping age distributions with Ahuriri Lagoon records (Fig. 3) (Clark et al., 2019; Cochran et al., 2006; Pizer et al., 2022). None of the rapid subsidence events at Ahuriri Lagoon correlate with the preserved Holocene uplift events at Cape Kidnappers, as would be expected from a nearby upper plate fault earthquake, though this could be due to incomplete preservation at either site (Hull, 1987). The age of one Ahuriri Lagoon subsidence event does overlap with terrace uplift at Waimārama at c. 5 ka (Fig. 3) (Clark et al., 2019; Pizer et al., 2022).

Longer term (c. 400 ka) subsidence near Ahuriri Lagoon is recorded in the numerous forearc basins in offshore and near-shore Hawke's Bay; these basins (e.g., the Kidnappers Basin) are located between active thrust-fault-controlled ridges and develop in response to changes in climate, sedimentation, and tectonic processes (Fig. 1c) (e.g., Dravid and Brown 1997, Paquet et al, 2011). The basin-scale records are too coarse to resolve individual earthquake histories, but indicate that cumulative fault displacements follow expected upper plate fault deformation patterns (i.e., hanging wall uplift and footwall subsidence; Fig 2), and across the Awanui fault, mimic the 1931 event displacement profile (e.g., Begg et al., 2022; Dravid and Brown 1997; Hull 1986).

238 ### 2.5 Upper plate faults

239 The active offshore and nearshore faults in Hawke's Bay are generally characterized as
240 out-of-sequence thrust faults that maintain the accretionary wedge taper (Fig. 1c) (Barnes et al.,
241 2010). Published seismic survey data indicate the presence of predominantly northwest-dipping
242 listric faults, which result from reactivation of extensional faults preceding the current
243 convergent regime (Fig. 1b) (Barnes et al., 2010; Barnes & Nicol, 2004). The fault tips are
244 generally buried in the near-surface below anticline ridges that are separated by sedimentary
245 basins (e.g., Barnes et al., 2002; Paquet et al., 2011; Paquet et al., 2009). Southeast-dipping
246 backthrusts are relatively shallow features (i.e. limited to the upper few kilometers) that splay
247 from the primary northwest-dipping structures (e.g., Barnes et al., 2002; Paquet et al., 2011;
248 Paquet et al., 2009), and are therefore unlikely to be independently seismogenic.
249 The Lachlan fault is the best-characterized, fastest slipping fault in Hawke Bay (Fig. 1c)
250 (Barnes et al., 2002; Mountjoy & Barnes, 2011). Depth-corrected seismic profiles suggest a
251 listric shape, steep dips (55–70°) in the upper 1–2 km, and gentle dips (15–20°) from 7–8 km
252 depth to the subduction zone interface (Barnes et al., 2002; Mountjoy & Barnes, 2011). Full
253 rupture of the Lachlan fault (79 km length) could produce an earthquake with c. M_w 7.7–8.0,
254 while rupture along only the fastest slipping segment is estimated at c. M_w 7.6–7.8 (Barnes et al.,
255 2002).
256 Farther south are the Waimārama, Kairākau, and Kidnappers Ridge faults (Fig. 1c) (e.g.,
257 Paquet et al., 2011). Kidnappers Ridge is a zone of uplifted and folded sea floor that is cored by
258 several active but unnamed northwest-dipping, listric reverse faults and a southeast dipping
259 backthrust (the Kidnapper's fault) (Fig. 1c) (Barnes et al., 2002). The northwest-dipping faults
260 likely continue along strike under Cape Kidnappers, though the surface expression there is less
261 clear and the fault tip may be buried (Fig. 1c) (Paquet et al., 2011). The Waimārama-Kairākau
262 thrust faults dip steeply northwest in the near-surface and are inferred to be listric, similar to
263 other nearby faults, but cannot be imaged at depth by marine surveys (Fig. 1c) (Mountjoy &
264 Barnes, 2011).
265 Mapped onshore faults located near Napier (e.g., Awanui, Tukituki, and similar faults)
266 dip steeply northwest in the near-surface and accommodate oblique dextral-reverse slip (Fig. 1c)
267 (Begg et al., 2022; Kelsey et al., 1998; Lee et al., 2020; McGinty et al., 2001). These faults likely
268 produce coseismic uplift at Ahuriri Lagoon; any subsidence would be southeast within their
269 respective footwalls, as observed in 1931, or much farther inland (Figs. 1, 2) (Haines & Darby,
270 1987; Hull, 1990; McGinty et al., 2001). This is consistent with the long-term geologic record
271 which shows Kidnappers basin growth in the Awanui fault footwall (Begg et al. 2022; Dravid
272 and Brown, 1997).
273 The rake for these upper plate faults is poorly constrained. Due to the obliquity of plate
274 convergence compared to fault strike, these faults likely contain a variable component of dextral
275 slip (Fig. 1) (e.g., Barnes et al., 2002; Barnes & Nicol, 2004). Thus, reported dip-slip and vertical
276 separation rates represent a minimum of the full slip rate or single-earthquake slip values.
277 Finally, the Community Fault Model includes simplified versions of the Kidnappers
278 Ridge, Waimārama, and Kairākau faults, represented with planar 40 ± 10º northwest dips and a
279 90 ± 20º rake (reverse motion) (Seebeck et al., 2022). How these simplifications (i.e., shape, slip
280 distribution, dip angle, and rake) might affect expected coastal displacements and hazard
281 assessments remains untested.

2.6 Previous elastic dislocation modeling

Previous studies used forward elastic dislocation models to estimate tsunami hazard or to determine source faults for historic earthquake and paleoseismic records along the central Hikurangi margin (Cochran et al., 2006; Fraser et al., 2014; Hayward et al., 2016; Litchfield et al., 2022; McGinty et al., 2001). The 1931 Napier earthquake coseismic surface deformation was fit using steep planar faults, rupture from 5 km depth to the interface, and up to 8 m each of dextral and reverse slip (Haines & Darby, 1987; McGinty et al., 2001).

Cochran et al. (2006) investigated sources for subsidence at Te Paeroa and Opoho and uplifted terraces at Mahia Peninsula (Fig. 3). Results indicated that both a gently dipping Lachlan fault and subduction interface sources could contribute to uplift and subsidence there, either synchronously or separately, but subduction rupture was required for the larger subsidence (>0.9 m) records (Cochran et al., 2006). Fraser et al. (2014) presented forward elastic dislocation models of the Lachlan fault and subduction interface to estimate tsunami inundation hazard at Napier. Those Lachlan fault scenarios used a planar, steep fault (60º dip) and uniform slip that resulted in negligible hanging wall and coastal subsidence. The subduction rupture followed interface geometry (i.e., not planar) with a slip distribution informed by contemporary coupling patterns; several central margin rupture scenarios (M_w 8.2–8.4) and multi-segment scenarios (M_w 8.8–9.0) result in subsidence between 0.3 and 0.6 m near Napier (Fraser et al., 2014).

Litchfield et al. (2022) showed that reverse slip on the Kairākau fault could produce observed meter-scale terrace uplift at Aramoana, and potentially other coastal sites, but subsidence from that fault did not reach Ahuriri Lagoon. Hayward et al. (2016) provided one subduction interface elastic dislocation model that produces subsidence at Ahuriri Lagoon and the Hawke's Bay coastline, but provided no information on the earthquake source parameters or magnitude. None of the existing dislocation models explore subsidence at Ahuriri Lagoon from smaller subduction interface earthquakes (<M_w 8.2) or closer offshore upper plate faults.

3 Elastic dislocation modeling methods

We used elastic dislocation models to test whether recognized upper plate fault and subduction interface sources could produce recorded subsidence (≥0.5 m) at Ahuriri Lagoon. The models focus on the Kidnappers Ridge, Waimārama, and Kairākau upper plate faults because these structures have gentle dips at depth and likely extend near or below Ahuriri Lagoon, and are thus capable of producing subsidence there (e.g., Fig. 2c). Closer faults (e.g., Awanui and Tukituki faults) are likely to produce uplift at Ahuriri Lagoon based on the proximal hanging wall location, as seen in the 1931 earthquake (Fig. 1c, Fig 2b, 2c) (Hull, 1990; Haines & Darby, 1987; McGinty et al., 2001). There are no mapped, active, northwest-dipping reverse faults northwest of Ahuriri Lagoon that could produce coseismic footwall subsidence there.

We also modeled displacements from several possible subduction zone rupture scenarios. Those elastic dislocation models explore how slip location on the interface affects coseismic subsidence at Ahuriri Lagoon and whether those slip distributions reflect modern coupling.

3.1 Upper plate fault elastic dislocation models

We present two upper plate fault model geometries: a listric fault based on seismic survey data and a planar fault as represented in the Community Fault Model (Seebeck et al., 2022). Both listric and planar fault geometries use the same simplified trace of the combined Kidnappers Ridge, Waimārama, and Kairākau faults with a strike of 227º and total fault length of 75 km.

Fault length is based on the distribution of mapped fault traces, which could conceivably link during an earthquake, and the 80-km-long Napier earthquake rupture (McGinty et al., 2001). All upper plate scenarios use 8 m peak slip, informed by average earthquake dip-slip estimates on the Lachlan fault (5–9 m for single segment, 4–7 m for multi segment) (Barnes et al., 2002) and the dislocation modelling discussed above in Section 2.5 (Cochran et al., 2006; Fraser et al., 2014; McGinty et al., 2001).

The planar upper plate fault model dips uniformly at 40º from the surface to the subduction interface at 15.7 km depth. The listric upper plate fault model dips change from 80º at 0–1 km depth to 22º at 6 km depth, and continues at 22º from 6 to 21 km depth (to the intersection with the interface). For both upper plate fault shapes, we test whether allowing additional slip on the subduction interface (up to 3 km depth) affects the slip distribution and deformation pattern. Since rake is not well constrained, all upper plate dislocation models are run twice: once with pure reverse rake (90º rake) and again with oblique reverse-dextral rake (135°).

Model geometries were discretized into 3 km by 3 km patches. Green's functions representing vertical displacements at Ahuriri Lagoon for 1 m of slip on each patch were calculated using the method of Okada (1985), assuming a Poisson ratio (ν) of 0.25.

We use a combination of slip inversions and forward models to investigate the plausibility of subsidence at Ahuriri Lagoon due to upper plate earthquakes. Our inversions solve for slip distributions on upper plate faults that maximize subsidence at the lagoon. We emphasize that there is no unique solution to this inversion — clearly, the range of values of single-event vertical motions at a single site cannot constrain the 3,600 parameters required to define a slip distribution on our modelled listric fault, even if the uncertainty in this geometry is ignored. The inversion results are highly sensitive to specified fault geometry, rake, maximum slip, and smoothing parameters, but are useful for, but are useful for three reasons. First, they test whether an upper-plate earthquake could cause subsidence at Ahuriri Lagoon, although that test could also be done using forward models. Second, they help identify the optimal location for slip that promotes subsidence of Ahuriri Lagoon (within the constraints of the parameters above). It would be possible to search for this optimal location using a grid search or forward models and a trial-and-error approach; however, our inversions allow for more freedom in the shape of the slip distribution than these other approaches. Third, inverting for slip allows us to estimate an approximate maximum magnitude for subsidence, again assuming the orientation, smoothness and maximum magnitude of slip.

Since there are few constraints on slip distributions that could cause subsidence at Ahuriri Lagoon, we also run a suite of forward models to investigate the sensitivity of vertical motions at the lagoon to different parameters, including slip taper width, down-dip extent, and up-dip extent. The forward models use the same fault geometry as the inversion and hold all other parameters the same in each trial (further details in Data Repository Text S1).

The inversions used the pygmo (Biscani & Izzo, 2020) and NLopt (http://github.com/stevengj/nlopt) libraries, monotonic basin hopping and SLSQP algorithms (Kraft, 1988; Wales & Doye, 1997), and l^2-norm minimization. We experimented with different relative weights for Laplacian smoothing and penalized slip on all the modelled fault edges. This slip taper also approximates a buried fault rupture tip, where slip is zero along the top 3 km of the fault (i.e., one tile length), consistent with 1931 Napier earthquake modeled slip and fault propagation folds beneath Cape Kidnappers and in Hawke Bay (Barnes & Nicol, 2004; Haines & Darby, 1987; McGinty et al., 2001).

3.2 Subduction interface elastic dislocation models

We used forward elastic dislocation models to investigate if subduction interface earthquakes, informed by modern coupling and slow-slip event locations, produce subsidence at Ahuriri Lagoon. Wallace et al. (2020) show that over decadal timescales, the central Hikurangi interface has low coupling (i.e., is creeping). However, between slow-slip events on annual timescales, the slow-slip source areas are more coupled (Wallace et al., 2020). We therefore test rupture patches that only include the shallow, more permanently locked interface as well as those that include the slow-slip source area. We also tested slip on the interface patches located between slow-slip events, which may be partially or heterogeneously coupled based on vertical derivative of horizontal strain data (Dimitrova et al., 2016; Wallace, 2020). Finally, we estimate the location and slip patch for the smallest interface earthquake capable of producing 0.5 m subsidence at Ahuriri Lagoon, irrespective of the modern coupling data.

We calculated surface displacements using the method of Nikkhoo & Walter (2015) and the Poisson ratio above (0.25). The interface is represented by a triangular mesh surface with 3 km triangles that follows geometry of Williams et al. (2013). The scenarios used average slip that follows the magnitude-area scaling relationship from Stirling et al., (2021) with a C value of 4.0 (Gerstenberger et al., 2022). Interface slip tapers to zero over 12 km to the patch edge (approximately matching upper plate fault inversion taper). The rake for each subduction interface patch is from Wallace et al. (2012).

4 Elastic dislocation modeling results

The paleoseismic subsidence records at Ahuriri Lagoon provide minimum constraints on coastal deformation preservation potential (Fig. 3). The eight documented coseismic subsidence events range from 0.5 – 1.2 m (average 0.85 m) subsidence, and the smallest subsidence is estimated at 0.5 m ± 0.5 m (Hayward et al. (2015). These values are similar to subsidence documented at Te Paeroa and Opoho, where the smallest measured coseismic subsidence was c. 0.5 – 1.0 m and the largest subsidence was c. 1.0 – 2.0 m (Cochran et al., 2006), and at Pakuratahi Valley, with >0.5 m estimated coseismic subsidence (Fig. 3) (Pizer et al., 2022). It is therefore probable that subsidence events <0.5 m would not be reliably preserved in the geological record at Ahuriri Lagoon, and we adopt c. 0.5 m as a minimum threshold.

4.1 Upper plate fault inversion model results

Both the modelled listric and planar fault geometries can produce subsidence of at least 0.5 m at Ahuriri Lagoon with reasonable slip magnitudes and distributions (Fig. 4). The listric fault inversion models produce 0.73 m and 0.72 m subsidence for reverse and oblique rakes, respectively, without any slip on the subduction interface. The resulting earthquake magnitudes are M_w 7.7 (Fig. 4). Allowing additional slip on the subduction interface increased the maximum subsidence to 0.96 m for the oblique rake model, but did not increase subsidence for the pure reverse rake model (Fig. S2).

For the planar fault, subsidence at Ahuriri Lagoon only occurs when slip continues onto the subduction interface. This results in subsidence of 0.61 m and 0.48 m with reverse and oblique rakes, respectively, and results in a magnitude of M_w 7.6 (Fig. 4c) (see supplement for additional results). Higher average fault dip compared to the listric fault models contribute to slightly larger uplift values given the same rake (Fig. 2).

In all upper plate fault models, variations in rake influence the spatial pattern of surface deformation. Oblique slip shifts peak subsidence southwest (i.e., opposite the direction of rake) and peak uplift northeast compared to pure reverse rake (Fig. 4, S4, S5).

In addition to rake, the location of peak uplift and subsidence, and thus our modeled subsidence at Ahuriri Lagoon, is dependent on the extent of slip at depth. We reiterate that these subsidence values and exact locations are non-unique results (Figs. S4, S5). However, the inversion results demonstrate that sizeable subsidence from upper plate faults is plausible and consistent with a range of slip distributions and geometries. We explore those results in more detail below.

4.2 Sensitivity of subsidence at Ahuriri Lagoon to modelled slip distribution

The forward models demonstrate how certain inversion parameter choices (i.e., slip taper; up-dip, down-dip, and lateral slip extent) might change our findings (Figs. S4-S8; additional details in Text S1). Changing the up-dip slip extent only affects subsidence insofar as it changes the overall slip area, and thus maximum displacement. These effects are negligible for subsidence Ahuriri Lagoon in our models (Fig. S3). The down-dip slip extent model variations show that subsidence is largest at Ahuriri Lagoon when slip terminates underneath, or just up-dip of, Ahuriri Lagoon (Figs. S6-S8). The range of subsidence values at Ahuriri Lagoon is small (c. 0.2 m) for ruptures that terminate between 9 km up-dip and 9 km down-dip of upper plate-interface intersection, given the same slip taper width (Figs. S6-S8). The slip taper width (i.e., how sharply slip tapers) affects Ahuriri Lagoon subsidence by moving the peak slip values, and thus peak subsidence, closer or father away (e.g., compare part d for Figs. S6-S8). For the same down-dip slip extent, our taper widths (9 km, 15 km, and 21 km) change Ahuriri Lagoon displacement by <0.2 m.

Variations in along-strike rupture extent result in translations of surface displacement. The resulting changes in subsidence at Ahuriri Lagoon are more pronounced for oblique rakes because maximum subsidence is not orthogonal to fault strike (Fig. S4, S5). In the oblique rake inversion model, for example, slip is primarily east of the lagoon to maximize subsidence at the lagoon (Fig. 4). If slip instead extends along the entire modeled fault, peak slip is shifted southwest and Ahuriri Lagoon subsidence is slightly reduced (Fig. S5). This relationship is also why additional slip on the interface results in greater subsidence at Ahuriri Lagoon for oblique rakes, but not for pure reverse rake (Fig. S2).

The individual effects of slip taper, down-dip slip terminations, and lateral slip terminations are relatively minor and lend confidence that our interpretations based on inversion results are valid. Together, they indicate that a rupture that terminates or has peak slip far away from Ahuriri Lagoon (e.g., Fig. S6a, S8d) will be less likely to produce subsidence ≥0.5 m at Ahuriri Lagoon. In other words, if earthquakes on these upper plate faults terminate at especially shallow or deep depths rather than near upper plate fault-interface transition, or too far away along strike, subsidence may not be large enough to be preserved at Ahuriri Lagoon. Conversely, they indicate that there are a wide range of slip distributions capable of producing subsidence ≥0.5 m at Ahuriri Lagoon.

4.3 Subduction interface model results

In our subduction interface forward models, subsidence did not exceed 0.5 m at Ahuriri Lagoon when slip was constrained by the locked, partially locked, or shallow slow-slip event extents, even at great magnitudes ($\geq M_w$ 8.5) (Fig. 5a–b). The subduction interface rupture

scenarios only produce subsidence ≥ 0.5 m at Ahuriri Lagoon when the down-dip termination of the slip patch is approximately below Ahuriri Lagoon (Fig. 5c–d, S9). Importantly, that part of the interface is between slow-slip patches and in a zone that is considered creeping over decadal timescales (Wallace, 2020); it does however overlap with a possible smaller locked interface patch shown by Dimitrova et al. (2016). Our smallest subduction interface rupture that produced ≥ 0.5 m subsidence at Ahuriri Lagoon had a magnitude of M_w 7.6 (Fig. 5d). Both uplift and subsidence from the M_w 7.6 scenario diminish to near-zero over a short distance (c. 50 km).

These rupture scenarios are not exhaustive or predictive, but take into consideration how interface slip extent translates to surface deformation and the minimum requirements to produce sizable coastal subsidence. Different magnitude events or alternative slip distributions will change the absolute vertical deformation values, but the overall patterns would remain similar. Even a whole-margin rupture (i.e., c. M_w 9.0) will not produce significant subsidence at Ahuriri lagoon if slip only occurs within the currently fully coupled portions of the interface.

5 Discussion

5.1 Can slip on upper plate faults cause subsidence at Ahuriri Lagoon?

Our results demonstrate that both upper plate fault and subduction interface earthquakes may produce coseismic subsidence of at least 0.5 m at Ahuriri Lagoon. These scenarios fit within the known fault and slip parameters and suggest that coseismic subsidence at Ahuriri lagoon can be produced from several fault sources and rupture scenarios.

For the elastic dislocation models presented here, the greatest Ahuriri Lagoon subsidence is caused by a gently dipping fault with a slip patch southeast (i.e., on the up-dip side) of Ahuriri Lagoon. Our results also imply that multi-fault or multi-segment ruptures on the Kidnappers Ridge, Waimārama, and Kairākau fault systems are required to produce similar-sized or larger earthquakes (Fig. 1). How these structures may link at depth remains unknown, but given the similarity in orientation, close proximity, and short steps between fault traces, it is reasonable that these faults may rupture together (e.g., Clark et al., 2017; Litchfield et al., 2022). If the upper plate faults are significantly steeper at depth than considered here, or have moderate dips and do not rupture with the subduction zone interface, then surface displacement may be dominated by uplift (e.g., Fig. 2a).

Earthquakes smaller than c. M_w 7.5 may not produce enough subsidence for preservation in the lagoons, though smaller amounts of coastal subsidence would still present significant coastal hazard and risk. The estimated magnitude for a full Lachlan fault rupture is M_w 7.8-8.0 (Barnes et al., 2002; Mountjoy & Barnes, 2011); the Kidnappers Ridge, Waimārama, and Kairākau faults are less well characterized but their similar geometry suggests comparable earthquake potentials. If these faults rupture with the subduction interface, their potential earthquake magnitudes could be greater.

5.2 Are subduction earthquakes required to explain the Ahuriri Lagoon record?

We have shown that upper plate faults can cause subsidence at Ahuriri Lagoon, but here we consider whether known faults in Hawke Bay have fast enough slip rates, short enough recurrence times, or large enough earthquake slip to account for all Holocene geologic subsidence records at Ahuriri Lagoon.

Ahuriri Lagoon records eight rapid subsidence events over the last c. 7 ka with an average inter-event time of 900 yr and net tectonic subsidence of c. 8–9 m (prior to the 1931 CE

earthquake) (Fig. 3) (Hayward et al., 2016; Hull, 1986). Our simplified upper plate fault elastic dislocation models produce an average 4 m slip per earthquake, similar to models of the 1931 Napier event. For a minimum slip rate of 2.0 mm/yr on the Kidnappers Ridge-Waimārama faults (see justification in Text S1), this corresponds to an average recurrence interval of 2,000 yrs. This is a crude estimate; coseismic displacement distributions and sedimentary environment conditions mean not all earthquake subsidence may be recorded (resulting in a longer apparent recurrence interval), while the minimum slip rate means earthquakes may have a shorter recurrence interval. Despite these caveats, the substantial difference between the c. 900 yr average inter-event time recorded at Ahuriri Lagoon and the 2,000 yr estimated upper plate fault recurrence interval range shows some additional source other than upper plate faults is likely needed to produce all subsidence events recorded at Ahuriri Lagoon. Barring an unmapped, fast-slipping upper plate fault, the subduction interface is the most feasible alternate contributor to subsidence at Ahuriri Lagoon. Alternatively, faults may have temporally variable slip rates or exhibit earthquake clustering.

In the paleoseismic record, there is only one interpreted earthquake that potentially indicates synchronous coseismic marine terrace uplift and lagoon subsidence near Napier (Fig. 3) (Clark et al., 2019; Pizer et al., 2022). This possible event is recorded by 0.5 m ± 0.5 m rapid (i.e., coseismic) subsidence at Ahuriri Lagoon at 5,205–4,625 cal yr B.P (Clark et al., 2019; Hayward et al., 2016), rapid subsidence at Pakuratahi Valley at 4,837–4,584 cal yr B.P. (Pizer et al., 2022), and 3.5 m of terrace uplift at Waimārama at 5,030–4,490 cal yr B.P (Fig. 3) (Clark et al., 2019; Miyauchi et al., 1989). The overlap between these records could suggest the same earthquake at all sites, or multiple closely timed events. If these records are from a single event, the deformation fits the expected uplift and subsidence profile from an upper plate fault source (Fig. 3).

The lack of other correlating paleoearthquakes across all sites is perhaps not surprising given that vertical deformation from upper plate sources is more sensitive to the slip patch location and rake than a larger subduction interface event. It is possible that some upper plate fault earthquakes may not generate both a subsidence record and uplifted terrace due to a non-optimal slip patch. Alternatively, coastal erosion and sea level rise may remove marine terrace evidence while better preserving subsidence (e.g., Dura et al., 2016; Hull 1987).

An alternative way to distinguish Ahuriri Lagoon paleoearthquake sources is through the magnitude and extent of subsidence, since subduction earthquakes are capable of producing larger and more widespread coseismic subsidence than upper plate faults (Fig. 2). At Ahuriri Lagoon, most event subsidence is c. 0.5–1.0 m, but two Ahuriri Lagoon paleoearthquakes show subsidence ≥ 1.0 m (1.0 ± 0.3 m and 1.2 ± 0.4 m; Hayward et al., 2016). In our elastic dislocation models, only larger magnitude ($>M_w$ 8.0) interface earthquakes were capable of maximum hanging wall subsidence ≥ 1 m (Fig. 5, S9). Larger subsidence events may be more reasonably explained by a subduction interface source (or combination upper plate and subduction) than upper plate faults alone, similar to conclusions from Te Paeroa and Opoho (Fig. 3) (Cochran et al., 2006). Additionally, several of the Ahuriri Lagoon records have been correlated elsewhere along the margin, suggesting a larger source with broader deformation (Clark et al., 2019). However, the age control on these events can span hundreds of years and it is difficult to distinguish between closely timed, smaller earthquakes and more widespread synchronous deformation.

5.3 Megathrust slip behavior through multiple seismic cycles

The subduction interface scenarios constrained by the contemporary locked or partially locked interface do not produce sizable subsidence at Ahuriri Lagoon (Fig. 5). If any of the Ahuriri Lagoon paleoseismic subsidence events are from subduction earthquakes, as suggested by paleoseismic interpretations, they likely included slip on the interface currently dominated by creep (e.g., Fig. 5c, S9). Spatial heterogeneity in coupling on the central Hikurangi interface may provide a mechanism for deeper subduction slip and coseismic coastal subsidence (e.g., Dimitrova et al., 2016). Whether these potentially locked patches rupture in smaller earthquakes, or include more of the interface in larger events, remains unknown.

The mismatch between low modern coupling and paleoseismic evidence has also been noted along the Aleutian margin (Kelsey et al., 2015; Witter et al., 2019), with proposed explanations such as transient interseismic coupling over one or more seismic cycles, heterogeneous megathrust rupture properties, non-megathrust fault sources for tsunami deposits, or dynamic rupture processes. Dynamic weakening can cause slip into creeping segments of a fault when an earthquake initiates in a more locked section (Noda & Lapusta, 2013). Temporally variable coupling has been observed on the Chilean and Sumatran subduction zones over multi-year and decadal time scales when previous ruptures enhance shear stress on adjacent interface patches (Loveless, 2017; Melnick et al., 2017; Philibosian et al., 2017). However, the slow-slip and creeping behavior on the central Hikurangi subduction zone appears correlated to the interface roughness, subducting sediment composition and supply, and other more long-lived conditions, and therefore may not change over relatively short geologic time intervals (Gao and Wang, 2014; Gase et al., 2022). Additional monitoring is needed to evaluate the spatial and temporal variability in coupling on the Hikurangi subduction zone.

In light of our results, other proxies that inform our understanding of the seismic cycle of subduction zones should account for potential upper plate faulting. For example, coral microatolls are one of the most important ways of tracking coupling and subduction zone behaviour through time (e.g., Mallick et al., 2021; Meltzner et al., 2015; Philibosian et al., 2017). At a minimum, upper plate faulting may add noise to signals that have previously been attributed to subduction zone processes; in margins with significant upper plate faulting, previous interpretations may need re-evaluation to account for vertical deformation from non-subduction sources.

5.4 Tectonic contributions to present-day vertical land movements in Hawke's Bay

Modern geodetic data show the entire east coast of the North Island is subsiding with rates up to 5 mm/yr near Napier (Hamling et al., 2022). Elastic earthquake behavior suggests that coseismic subsidence here should be the counterpart of gradual interseismic uplift (Savage, 1983; Sieh et al., 1999; Wesson et al., 2015). Over multiple earthquake cycles, long-term vertical deformation should be near zero from the subduction interface and distal offshore upper plate faults (i.e., Waimārama, Kairakau, and Kidnapper Ridge faults) (e.g., Briggs et al., 2008), or slightly positive from the nearby Awanui fault (Fig. 1). Instead, Ahuriri Lagoon shows c. 8–9 m net tectonic subsidence over the Holocene (Hayward et al., 2016).

These apparently conflicting data suggest the central Hikurangi margin does not fit with the conventional seismic cycle model of coseismic recovery of interseismic strain accumulation. Other factors besides elastic and creeping subduction cycle strain recovery, such as groundwater removal and sediment compaction (Naish et al., 2022), may contribute to subsidence over 10^1 – 10^3 yr timescales.

5.5 Earthquake and tsunami hazard implications

The sizable subsidence difference between the listric and planar upper plate fault models presented here highlight that simplifying fault geometry may be adequate for some hazard applications (e.g., ground shaking), but underestimate hazard for other applications (e.g., displacement hazards) (Fig. 4). A gentler fault dip increases the maximum possible rupture width and affects the expected location and amount of surface deformation (Barnes et al., 2002). Thus, displacement-based hazard models should incorporate more realistic fault geometries or values that better represent dips at depth.

Fault source geometry can affect tsunami inundation because lower dips produce more coastal subsidence and thus greater flow depths and inundation extent. The previous tsunami inundation model for Napier overestimates dip on the Lachlan fault and therefore underestimates subsidence, though coseismic subsidence at Napier is likely minimal from that fault (Fraser et al., 2014). The Kidnappers Ridge, Kairākau, and Waimārama fault sources were not investigated in the previous tsunami inundation model for Napier, but produce up to c. 0.7 m subsidence at Napier in our models. However, these faults are included as fault sources in the National Tsunami Hazard Model that estimate wave heights along a fixed coastline (Power, 2013). The wave height models incorporate uncertainties by modelling a larger-than-expected event, and are thus less susceptible to underestimations caused by fault geometry (Power, 2013).

In addition to fault geometry, modeled rake clearly impacts the spatial distribution of uplift and subsidence (Fig. 4) and is therefore an important parameter in displacement hazard analyses. We note that the Community Fault Model rake (90 ± 20º) gives equal probability of a minor sinistral or dextral component of slip (Seebeck et al., 2022). A more realistic rake range for faults in Hawke Bay based on the oblique orientation to convergence is 90–135º, which spans from pure reverse to equal parts reverse and dextral slip (Fig. 1).

The extent of subduction interface slip drastically affects expected earthquake size, deformation, and hazard potential. The New Zealand National Seismic Hazard Model (NZ NSHM) incorporates the subduction interface coupling distribution for estimating shaking hazard from the subduction zone (Van Dissen et al., 2022). Because the paleoseismic record in Hawke's Bay indicates past large earthquakes, and the modern coupling distribution shows almost no slip deficit (i.e., no coupling), the hazard model manually imposes a slip deficit of 20% to the central Hikurangi margin. Therefore, resolving the relationship between earthquakes on upper plate faults and the subduction interface has direct implications for the NZ NSHM and downstream policies. Our new insights into upper plate faults as a cause of subsidence at Ahuriri Lagoon may justify reducing the influence of the Ahuriri record on the imposed slip deficit in future revisions of the NZ NSHM.

5 Conclusions

Understanding potential fault sources directly affects hazard planning and mitigation efforts. Hazards from ground motions, coastal vertical deformation, and tsunami — exacerbated by ongoing sea-level rise worldwide — vary greatly between great subduction earthquakes and upper plate faults. Elastic dislocation modelling of upper plate fault and subduction interface earthquakes provides a means to test possible sources for repeated coseismic subsidence at Ahuriri Lagoon near Napier, Aotearoa New Zealand. We find that both sources can produce subsidence ≥ 0.5 m at Ahuriri Lagoon. Our preferred upper plate fault source scenarios include more accurate listric fault geometry with gentle dips based on seismic reflection data. Simpler

fault models that use steeper, planar faults do not result is coastal subsidence and are likely inadequate for modeling coastal deformation in this setting.

The modeling results, along with slip rate and recurrence data, suggest that at least some of the eight paleoseismic subsidence events at Ahuriri Lagoon since 7 ka could be caused by slip on upper plate structures. This result deviates from many interpretations of coastal subsidence records, both in New Zealand and along other subduction margins, where megathrust events are typically the default source without significant evidence to the contrary. In Hawke's Bay, the upper plate structures may be important drivers of coseismic subsidence and should be considered as possible sources for the paleoseismic records there.

Our subduction earthquake model scenarios also showed that interface earthquakes only caused sizeable subsidence at Ahuriri Lagoon when slip occurred on currently creeping parts of the interface. Paleoseismic data recording large single-event subsidence and margin-wide correlations suggest megathrust events have occurred in the past. This apparent discrepancy between expected and past earthquake behavior suggests that modern coupling patterns are either more spatially and temporally heterogeneous than modern measurements, or that earthquake rupture can include creeping portions of the interface.

Acknowledgments

We thank Kelin Wang, an anonymous reviewer, and the editor for their contributions to improving the manuscript. This research was funded by the University of Canterbury Mason Trust, QuakeCoRE, and the New Zealand Earthquake Commission (EQC). Partial support was provided by the New Zealand Ministry of Business, Innovation and Employment (MBIE) through the Hazard Risk Management program (Strategic Science Investment Fund, contract C05X1702).

Open Research

The supplement includes figures S1–S9, Tables S1–2, and Text S1 that provide additional model results, mapping method details, and fault slip rate estimate; these data will be available in an open access data repository following peer review. Lidar used for strandline mapping is sourced from the LINZ Data Service and licensed for reuse under CC BY 4.0 (Hawke's Bay Regional Council & Toitū Te Whenua Land Information New Zealand (LINZ), 2020). The 250 m Bathymetic data shown in figures (Mitchell et al., 2012) is available at the New Zealand Bathymetry database website (https://niwa.co.nz/our-science/oceans/bathymetry). Figures were made with Matplotlib version 3.6.2 (https://doi.org/10.5281/zenodo.7275322) (Hunter, 2007), available under the Matplotlib license at

https://matplotlib.org/, and Adobe Illustrator. Maps were made using QGIS v3.8.0. The Elastic Dislocation software associated used in this manuscript is published on GitHub (will add link upon successful review).

673 **Figure 1**. Tectonic setting of the Hawke's Bay region. (a) Plate boundaries and simplified
674 tectonic regimes of the North Island. Hawke's Bay is located near the transition from upper plate
675 accretionary wedge thrust faults to the North Island Dextral Fault System (NIDFS). (b) Cross-
676 section of the Hikurangi subduction zone with schematic upper plate faults. Little is known about
677 the subsurface geometry of coastal upper plate faults, but primary structures typically dip
678 northwest. (c) Major active faults and key paleoseismic sites near central Hawke's Bay.
679 Northwest-dipping faults typically control slip and continue to interface; southeast-dipping faults
680 are typically shallow back thrusts that splay from other faults (e.g., Paquet et al., 2009, 2011;
681 Mountjoy and Barnes, 2011). Data: bathymetric DEM, Mitchell et al. (2012); onshore DEM,
682 Landcare Research NZ Ltd. (2011), onshore faults, Langridge et al. (2016) and Lee et al. (2020);
683 offshore faults, Paquet et al. (2009, 2011) and Mountjoy and Barnes (2011); Hikurangi Plateau
684 thickness, Davy & Wood (1994); paleoseismic data, Clark et al. (2019) (and referenecs within).
685
686 **Figure 2**. Generalized vertical deformation from various fault sources, assuming simple uniform
687 reverse slip on (a) steeply dipping planar upper plate, (b) gently dipping upper plate, (c) listric
688 upper plate, and (d) subduction interface faults. Both upper plate faults and subduction zone
689 earthquakes can produce sizeable subsidence depending on interest location relative to the fault,
690 fault dip angle, and slip amount. Estimates are based on the method of Okada (1985).
691
692 **Figure 3**. Paleoseismic data in the Hawke's Bay region. (a) Coastal uplift and subsidence sites
693 with estimated per-event vertical deformation, where available. Long-term uplift rates are
694 derived from uplifted Pleistocene marine terraces. (b) Age data for rapid uplift (red) and
695 subsidence (blue) events attributed to paleoearthquakes, presented at 2σ (95%). Question marks
696 indicate suspected erosion and potentially missing uplifted Holocene terraces. Simplified fault
697 mapping from Mountjoy and Barnes (2011); Paquet et al. (2009, 2011). Paleoseismic data from
698 Clark et al. (2019) (and references within), Litchfield et al. (2022), and Pizer et al. (2022).
699
700 **Figure 4**. Select elastic dislocation model results for listric and planar upper plate faults (UPF)
701 (see Data Repository for additional results). These models have set geometry, rake, peak slip,
702 and slip taper conditions are inverted for the slip distribution that produces maximum subsidence
703 at Ahuriri Lagoon (A.L.). (a) The listric UPF with pure reverse motion and (b) listric UPF with
704 oblique motion both can produce at least 0.5 m of subsidence at Ahuriri Lagoon with reasonable
705 magnitudes and slip distributions. (c) The steeper, planar fault only produces 0.5 m subsidence at
706 Ahuriri Lagoon when substantial slip also occurs on the subduction interface. C.K. = Cape
707 Kidnappers. Grey contour interval = 1 m vertical displacement; blue dashed contour = -0.5 m
708 vertical displacement.
709
710 **Figure 5**. Forward elastic dislocation model results of subduction interface earthquakes. (a)
711 Interface earthquakes on the locked or partially locked Hikurangi margin results in offshore
712 subsidence but o subsidence at Ahuriri Lagoon (A.L.). Coupling boundary (grey dashed line)
713 from Wallace et al., (2012). (b) Earthquakes on the locked interface and adjacent, shallow slow-
714 slip event (SSE) extent do not produce significant subsidence at A. L. Teal dotted polygon = 20
715 mm cumulative slip contour from 2006–2008 SSEs; teal dashed polygons = 100 mm cumulative
716 slip contour from 2002–2014 SSEs (Wallace, 2020). (c) Slip between modern SSEs on the
717 currently creeping interface produces moderate subsidence at Ahuriri Lagoon. (d) Smaller
718 magnitude interface earthquakes can produce c. 0.5 m of subsidence at Ahuriri Lagoon with an

719 optimally located slip patch that terminates down-dip below Ahuriri Lagoon. C.K. = Cape
720 Kidnappers. Listric upper plate fault geometry used in the main text shown as a grey dashed line
721 in the cross sections.

References

Atwater, B. F. (1987). Evidence for great Holocene earthquakes along the outer coast of Washington state. *Science*, 236(4804), 942–944. https://doi.org/10.1126/science.236.4804.942

Atwater, B. F., & Hemphill-Haley, E. (1997). Recurrence intervals for great earthquakes of the past 3,500 years at northeastern Willapa Bay, Washington. *USGS Numbered Series* No. 1576; Professional Paper. http://pubs.er.usgs.gov/publication/pp1576

Barnes, P. M., Lamarche, G., Bialas, J., Henrys, S., Pecher, I., Netzeband, G. L., Greinert, J., Mountjoy, J. J., Pedley, K., & Crutchley, G. (2010). Tectonic and geological framework for gas hydrates and cold seeps on the Hikurangi subduction margin, New Zealand. *Marine Geology*, *272*(1–4), 26–48. https://doi.org/10.1016/j.margeo.2009.03.012

Barnes, P. M., & Nicol, A. (2004). Formation of an active thrust triangle zone associated with structural inversion in a subduction setting, eastern New Zealand. *Tectonics*, *23*(1), n/a-n/a. https://doi.org/10.1029/2002TC001449

Barnes, P. M., Nicol, A., & Harrison, T. (2002). Late Cenozoic evolution and earthquake potential of an active listric thrust complex above the Hikurangi subduction zone, New Zealand. *GSA Bulletin*, *114*(11), 1379–1405. https://doi.org/10.1130/0016-7606(2002)114<1379:LCEAEP>2.0.CO;2

Begg, J. G., Jones, K. E., Lee, J. M., & Tschritter, C. (2022). 3D geological model of the Napier-Hastings urban area [explanatory text]. https://doi.org/10.21420/QFEK-9369

Berryman, K. (1993a). Age, height, and deformation of Holocene marine terraces at Mahia Peninsula, Hikurangi Subduction Margin, New Zealand. *Tectonics*, *12*(6), 1347–1364. https://doi.org/10.1029/93TC01542

745 Berryman, K. (1993b). Distribution, age, and deformation of Late Pleistocene marine terraces at
746 Mahia Peninsula, Hikurangi Subduction Margin, New Zealand. *Tectonics*, *12*(6), 1365–
747 1379. https://doi.org/10.1029/93TC01543
748 Berryman, K., Clark, K., Cochran, U., Beu, A., & Irwin, S. (2018). A geomorphic and tectonic
749 model for the formation of the flight of Holocene marine terraces at Mahia Peninsula,
750 New Zealand. *Geomorphology*, *307*, 77–92.
751 https://doi.org/10.1016/j.geomorph.2017.10.014
752 Berryman, K., Ota, Y., Miyauchi, T., Hull, A., Clark, K., Ishibashi, K., Iso, N., & Litchfield, N.
753 (2011). Holocene Paleoseismic History of Upper-Plate Faults in the Southern Hikurangi
754 Subduction Margin, New Zealand, Deduced from Marine Terrace Records. *Bulletin of the*
755 *Seismological Society of America*, *101*(5), 2064–2087.
756 https://doi.org/10.1785/0120100282
757 Biscani, F., & Izzo, D. (2020). A parallel global multiobjective framework for optimization:
758 Pagmo. *Journal of Open Source Software*, 5(53), 2338.
759 https://doi.org/10.21105/joss.02338
760 Bosserelle, A. L., Morgan, L. K., & Hughes, M. W. (2022). Groundwater Rise and Associated
761 Flooding in Coastal Settlements Due To Sea-Level Rise: A Review of Processes and
762 Methods. *Earth's Future*, *10*(7). https://doi.org/10.1029/2021EF002580
763 Briggs, R. W., Engelhart, S. E., Nelson, A. R., Dura, T., Kemp, A. C., Haeussler, P. J., Corbett,
764 D. R., Angster, S. J., & Bradley, L.-A. (2014). Uplift and subsidence reveal a
765 nonpersistent megathrust rupture boundary (Sitkinak Island, Alaska). *Geophysical*
766 *Research Letters*, *41*(7), 2289–2296. https://doi.org/10.1002/2014GL059380

767 Briggs, R. W., Sieh, K., Amidon, W. H., Galetzka, J., Prayudi, D., Suprihanto, I., Sastra, N.,
768 Suwargadi, B., Natawidjaja, D., & Farr, T. G. (2008). Persistent elastic behavior above a
769 megathrust rupture patch: Nias island, West Sumatra. *Journal of Geophysical Research*,
770 *113*(B12), B12406. https://doi.org/10.1029/2008JB005684
771 Bruun, P. (1962). Sea-level rise as a cause of shore erosion. *Journal of the Waterways and*
772 *Harbors Division*, *88*(1), 117–130.
773 Chlieh, M., Avouac, J. P., Sieh, K., Natawidjaja, D. H., & Galetzka, J. (2008). Heterogeneous
774 coupling of the Sumatran megathrust constrained by geodetic and paleogeodetic
775 measurements. *Journal of Geophysical Research*, *113*(B5), B05305.
776 https://doi.org/10.1029/2007JB004981
777 Chlieh, M., Perfettini, H., Tavera, H., Avouac, J.-P., Remy, D., Nocquet, J.-M., Rolandone, F.,
778 Bondoux, F., Gabalda, G., & Bonvalot, S. (2011). Interseismic coupling and seismic
779 potential along the Central Andes subduction zone. *Journal of Geophysical Research*,
780 *116*(B12), B12405. https://doi.org/10.1029/2010JB008166
781 Clark, K. J., Hayward, B. W., Cochran, U. A., Wallace, L. M., Power, W. L., & Sabaa, A. T.
782 (2015). Evidence for Past Subduction Earthquakes at a Plate Boundary with Widespread
783 Upper Plate Faulting: Southern Hikurangi Margin, New Zealand. *Bulletin of the*
784 *Seismological Society of America*, *105*(3), 1661–1690.
785 https://doi.org/10.1785/0120140291
786 Clark, K. J., Howarth, J., Litchfield, N., Cochran, U., Turnbull, J., Dowling, L., Howell, A.,
787 Berryman, K., & Wolfe, F. (2019). Geological evidence for past large earthquakes and
788 tsunamis along the Hikurangi subduction margin, New Zealand. *Marine Geology*, *412*,
789 139–172. https://doi.org/10.1016/j.margeo.2019.03.004

790 Clark, Kate J., Nissen, E. K., Howarth, J. D., Hamling, I. J., Mountjoy, J. J., Ries, W. F., Jones,
791 K., Goldstien, S., Cochran, U. A., Villamor, P., Hreinsdóttir, S., Litchfield, N. J.,
792 Mueller, C., Berryman, K. R., & Strong, D. T. (2017). Highly variable coastal
793 deformation in the 2016 MW7.8 Kaikōura earthquake reflects rupture complexity along a
794 transpressional plate boundary. Earth and Planetary Science Letters, 474, 334–344.
795 https://doi.org/10.1016/j.epsl.2017.06.048
796 Cochran, U., Berryman, K., Zachariasen, J., Mildenhall, D., Hayward, B., Southall, K., Hollis,
797 C., Barker, P., Wallace, L., Alloway, B., & Wilson, K. (2006). Paleoecological insights
798 into subduction zone earthquake occurrence, eastern North Island, New Zealand.
799 *Geological Society of America Bulletin*, *118*(9–10), 1051–1074.
800 https://doi.org/10.1130/B25761.1
801 Davy, B., & Wood, R. (1994). Gravity and magnetic modelling of the Hikurangi Plateau. *Marine*
802 *Geology*, *118*(1–2), 139–151. https://doi.org/10.1016/0025-3227(94)90117-1
803 Dimitrova, L., Wallace, L., Haines, A., & Williams, C. (2016). High-resolution view of active
804 tectonic deformation along the Hikurangi subduction margin and the Taupo Volcanic
805 Zone, New Zealand. *New Zealand Journal of Geology and Geophysics*, *59*(1), 43–57.
806 https://doi.org/10.1080/00288306.2015.1127823
807 Dravid, P. N., & Brown, L. J. (1997). Heretaunga Plains groundwater study: Volume 1-Findings.
808 Hawke's Bay Regional Council. https://www.hbrc.govt.nz/assets/Document-
809 Library/Projects/TANK/TANK-Key-Reports/Heretaunga-Plains-Groundwater-Study-
810 1997.pdf
811 Dura, T., Engelhart, S. E., Vacchi, M., Horton, B. P., Kopp, R. E., Peltier, W. R., & Bradley, S.
812 (2016). The role of Holocene relative sea-level change in preserving records of

subduction zone earthquakes. *Current Climate Change Reports*, *2*(3), 86–100. https://doi.org/10.1007/s40641-016-0041-y

Dura, T., Garner, A. J., Weiss, R., Kopp, R. E., Engelhart, S. E., Witter, R. C., Briggs, R. W., Mueller, C. S., Nelson, A. R., & Horton, B. P. (2021). Changing impacts of Alaska-Aleutian subduction zone tsunamis in California under future sea-level rise. *Nature Communications*, *12*(1), 7119. https://doi.org/10.1038/s41467-021-27445-8

Fraser, S. A., Power, W. L., Wang, X., Wallace, L. M., Mueller, C., & Johnston, D. M. (2014). Tsunami inundation in Napier, New Zealand, due to local earthquake sources. *Natural Hazards*, *70*(1), 415–445. https://doi.org/10.1007/s11069-013-0820-x

Gao, X., & Wang, K. (2014). Strength of stick-slip and creeping subduction megathrusts from heat flow observations. *Science*, 345(6200), 1038–1041. https://doi.org/10.1126/science.1255487

Gase, Andrew C., Bangs, Nathan L., Van Avendonk, Harm J. A., Bassett, Dan, & Henrys, Stuart A. (2022). Hikurangi megathrust slip behavior influenced by lateral variability in sediment subduction. *Geology*, 50(10), 1145–1149. https://doi.org/10.1130/G50261.1

Gerstenberger, M. C., Van Dissen, R. J., Rollins, C., DiCaprio, C., Chamberlain, C., Christophersen, A., Coffey, G. L., Ellis, S. M., Iturrieta, P., & Johnson, K. M. (2022). The Seismicity Rate Model for the 2022 New Zealand National Seismic Hazard Model. https://doi.org/10.21420/2EXG-NP48

Haines, A. J., & Darby, D. J. (1987). *Preliminary dislocation models for the 1931 Napier and 1932 Wairoa earthquakes* (114th ed.). New Zealand Geological Survey.

Hamling, I. J., Wright, T. J., Hreinsdóttir, S., & Wallace, L. M. (2022). A snapshot of New Zealand's dynamic deformation field from Envisat InSAR and GNSS observations

836 between 2003 and 2011. *Geophysical Research Letters*, *49*(2).
837 https://doi.org/10.1029/2021GL096465
838 Hawke's Bay Regional Council, & Toitū Te Whenua Land Information New Zealand (LINZ).
839 (2020). Hawke's Bay LiDAR 1 m DEM (2020). https://data.linz.govt.nz/layer/106487-
840 hawkes-bay-lidar-1m-dem-2020/
841 Hayward, B. W., Grenfell, H. R., Sabaa, A. T., Carter, R., Cochran, U., Lipps, J. H., Shane, P.
842 R., & Morley, M. S. (2006). Micropaleontological evidence of large earthquakes in the
843 past 7200 years in southern Hawke's Bay, New Zealand. *Quaternary Science Reviews*,
844 25(11–12), 1186–1207. https://doi.org/10.1016/j.quascirev.2005.10.013
845 Hayward, B. W., Grenfell, H. R., Sabaa, A. T., Clark, K. J., Cochran, U. A., & Palmer, A. S.
846 (2015). Subsidence-driven environmental change in three Holocene embayments of
847 Ahuriri Inlet, Hikurangi Subduction Margin, New Zealand. *New Zealand Journal of*
848 *Geology and Geophysics*, *58*(4), 344–363.
849 https://doi.org/10.1080/00288306.2015.1077872
850 Hayward, B. W., Grenfell, H. R., Sabaa, A. T., Cochran, U. A., Clark, K. J., Wallace, L., &
851 Palmer, A. S. (2016). Salt-marsh foraminiferal record of 10 large Holocene (last 7500 yr)
852 earthquakes on a subducting plate margin, Hawkes Bay, New Zealand. *Geological*
853 *Society of America Bulletin*, *128*(5–6), 896–915. https://doi.org/10.1130/B31295.1
854 Herman, M. W., & Furlong, K. P. (2021). Triggering an unexpected earthquake in an uncoupled
855 subduction zone. *Science Advances*, *7*(13), eabf7590.
856 https://doi.org/10.1126/sciadv.abf7590
857 Hull, A. G. (1985). *Late Quaternary geology of the Cape Kidnappers area: Hawke's Bay, New*
858 *Zealand* [Master's Thesis]. Victoria University of Wellington.

Hull, A. G. (1986). Pre-A.D. 1931 tectonic subsidence of Ahuriri Lagoon, Napier, Hawke's Bay, New Zealand. *New Zealand Journal of Geology and Geophysics*, *29*(1), 75–82. https://doi.org/10.1080/00288306.1986.10427524

Hull, A. G. (1987). A Late Holocene marine terrace on the Kidnappers Coast, North Island, New Zealand: Some implications for shore platform development processes and uplift mechanism. *Quaternary Research*, *28*(2), 183–195. https://doi.org/10.1016/0033-5894(87)90058-5

Hull, A. G. (1990). Tectonics of the 1931 Hawke's Bay earthquake. *New Zealand Journal of Geology and Geophysics*, *33*(2), 309–320. https://doi.org/10.1080/00288306.1990.10425689

Hunter, J. D. (2007). Matplotlib: A 2D Graphics Environment. *Computing in Science & Engineering*, 9(3), 90–95. https://doi.org/10.1109/MCSE.2007.55

Johnson, K. M., Wallace, L. M., Maurer, J., Hamling, I. J., Williams, C. A., Rollins, C., Gerstenberger, M. C., & Van Dissen, R. J. (2022). Geodetic deformation model for the 2022 update of the New Zealand National Seismic Hazard Model. *GNS Science Report*, 2021/37, 62. https://doi.org/10.21420/P93X-8293

Kaiser, A., Holden, C., Beavan, J., Beetham, D., Benites, R., Celentano, A., Collett, D., Cousins, J., Cubrinovski, M., Dellow, G., Denys, P., Fielding, E., Fry, B., Gerstenberger, M., Langridge, R., Massey, C., Motagh, M., Pondard, N., McVerry, G., … Zhao, J. (2012). The Mw 6.2 Christchurch earthquake of February 2011: Preliminary report. *New Zealand Journal of Geology and Geophysics*, *55*(1), Article 1. https://doi.org/10.1080/00288306.2011.641182

881 Kaneko, Y., Avouac, J.-P., & Lapusta, N. (2010). Towards inferring earthquake patterns from
882 geodetic observations of interseismic coupling. *Nature Geoscience*, *3*(5), 363–369.
883 https://doi.org/10.1038/ngeo843
884 Kelsey, H. M., Hull, A. G., Cashman, S. M., Berryman, K. R., Cashman, P. H., Trexler, J. H., Jr.,
885 & Begg, J. G. (1998). Paleoseismology of an active reverse fault in a forearc setting: The
886 Poukawa fault zone, Hikurangi forearc, New Zealand. *GSA Bulletin*, *110*(9), 1123–1148.
887 https://doi.org/10.1130/0016-7606(1998)110<1123:POAARF>2.3.CO;2
888 Kelsey, H. M., Ticknor, R. L., Bockheim, J. G., & Mitchell, E. (1996). Quaternary upper plate
889 deformation in coastal Oregon. *GSA Bulletin*, *108*(7), 843–860.
890 https://doi.org/10.1130/0016-7606(1996)108<0843:QUPDIC>2.3.CO;2
891 Kelsey, H. M., Witter, R. C., Engelhart, S. E., Briggs, R., Nelson, A., Haeussler, P., & Corbett,
892 D. R. (2015). Beach ridges as paleoseismic indicators of abrupt coastal subsidence during
893 subduction zone earthquakes, and implications for Alaska-Aleutian subduction zone
894 paleoseismology, southeast coast of the Kenai Peninsula, Alaska. *Quaternary Science*
895 *Reviews*, *113*, 147–158. https://doi.org/10.1016/j.quascirev.2015.01.006
896 Kraft, D. (1988). A software package for sequential quadratic programming. Forschungsbericht-
897 Deutsche Forschungs- Und Versuchsanstalt Fur Luft- Und Raumfahrt.
898 Landcare Research NZ Ltd. (2011). *NZDEM North Island 25 metre* [Data set]. Landcare
899 Research. https://doi.org/10.26060/6AS4-4Z82
900 Langridge, R., Ries, W., Litchfield, N., Villamor, P., Van Dissen, R., Barrell, D., Rattenbury, M.,
901 Heron, D., Haubrock, S., Townsend, D., Lee, J., Berryman, K., Nicol, A., Cox, S., &
902 Stirling, M. (2016). The New Zealand active faults database. *New Zealand Journal of*
903 *Geology and Geophysics*, *59*(1), 86–96. https://doi.org/10.1080/00288306.2015.1112818

Lay, T., & Nishenko, S. P. (2022). Updated concepts of seismic gaps and asperities to assess great earthquake hazard along South America. *Proceedings of the National Academy of Sciences*, *119*(51), e2216843119. https://doi.org/10.1073/pnas.2216843119

Lee, J. M., Begg, J. G., & Bland, K. J. (2020). *Geological map of the Napier-Hastings urban area*. https://doi.org/10.21420/XD8A-GS52

Litchfield, N. J., Morgenstern, R., Clark, K., Howell, A., Grant, G., & Turnbull, J. (2022). Holocene marine terraces as recorders of earthquake uplift: Insights from a rocky coast in southern Hawke's Bay, New Zealand. *Earth Surface Processes and Landforms*, esp.5496. https://doi.org/10.1002/esp.5496

Loveless, J. P. (2017). Super-interseismic periods: Redefining earthquake recurrence. *Geophysical Research Letters*, *44*(3), 1329–1332. https://doi.org/10.1002/2017GL072525

Loveless, J. P., & Meade, B. J. (2011). Spatial correlation of interseismic coupling and coseismic rupture extent of the 2011 M_W = 9.0 Tohoku-oki earthquake. *Geophysical Research Letters*, *38*(17), n/a-n/a. https://doi.org/10.1029/2011GL048561

Mallick, Rishav, Meltzner, Aron J., Tsang, Louisa L. H., Lindsey, Eric O., Feng, Lujia, & Hill, Emma M. (2021). Long-lived shallow slow-slip events on the Sunda megathrust. Nature Geoscience, 14(5), 327–333. https://doi.org/10.1038/s41561-021-00727-y

McGinty, P., Darby, D., & Haines, J. (2001). Earthquake triggering in the Hawke's Bay, New Zealand, region from 1931 to 1934 as inferred from elastic dislocation and static stress modeling. *Journal of Geophysical Research: Solid Earth*, *106*(B11), 26593–26604. https://doi.org/10.1029/2000JB000031

McNeill, L. C., Goldfinger, C., Yeats, R. S., & Kulm, L. D. (1999). The effects of upper plate deformation on records of prehistoric Cascadia subduction zone earthquakes. *Geological*

927 *Society, London, Special Publications*, *146*(1), 321–342.
928 https://doi.org/10.1144/GSL.SP.1999.146.01.19
929 Melbourne, T., Carmichael, I., DeMets, C., Hudnut, K., Sanchez, O., Stock, J., Suarez, G., &
930 Webb, F. (1997). The geodetic signature of the M8.0 Oct. 9, 1995, Jalisco Subduction
931 Earthquake. *Geophysical Research Letters*, 24(6), 715–718.
932 https://doi.org/10.1029/97GL00370
933 Melnick, D., Moreno, M., Quinteros, J., Baez, J. C., Deng, Z., Li, S., & Oncken, O. (2017). The
934 super-interseismic phase of the megathrust earthquake cycle in Chile. *Geophysical*
935 *Research Letters*, *44*(2), 784–791. https://doi.org/10.1002/2016GL071845
936 Meltzner, A. J., Sieh, K., Abrams, M., Agnew, D. C., Hudnut, K. W., Avouac, J.-P., &
937 Natawidjaja, D. H. (2006). Uplift and subsidence associated with the great Aceh-
938 Andaman earthquake of 2004. Journal of Geophysical Research: Solid Earth, 111(B2).
939 https://doi.org/10.1029/2005JB003891
940 Meltzner, A. J., Sieh, K., Chiang, H.-W., Shen, C.-C., Suwargadi, B. W., Natawidjaja, D. H.,
941 Philibosian, B., & Briggs, R. W. (2012). Persistent termini of 2004- and 2005-like
942 ruptures of the Sunda megathrust: SUNDA MEGATHRUST PERSISTENT
943 SEGMENTATION. *Journal of Geophysical Research: Solid Earth*, *117*(B4), n/a-n/a.
944 https://doi.org/10.1029/2011JB008888
945 Meltzner, A. J., Sieh, K., Chiang, H.-W., Shen, C.-C., Suwargadi, B. W., Natawidjaja, D. H.,
946 Philibosian, B. E., Briggs, R. W., & Galetzka, J. (2010). Coral evidence for earthquake
947 recurrence and an A.D. 1390–1455 cluster at the south end of the 2004 Aceh–Andaman
948 rupture. *Journal of Geophysical Research*, *115*(B10), B10402.
949 https://doi.org/10.1029/2010JB007499

950 Meltzner, A. J., Sieh, K., Chiang, H.-W., Wu, C.-C., Tsang, L. L. H., Shen, C.-C., Hill, E. M.,
951 Suwargadi, B. W., Natawidjaja, D. H., Philibosian, B., & Briggs, R. W. (2015). Time-
952 varying interseismic strain rates and similar seismic ruptures on the Nias–Simeulue patch
953 of the Sunda megathrust. Quaternary Science Reviews, 122, 258–281.
954 https://doi.org/10.1016/j.quascirev.2015.06.003
955 Ministry for the Environment. (2022). Interim guidance on the use of new sea-level rise
956 projections. ME 1667. Wellington: Ministry for the Environment.
957 https://environment.govt.nz/assets/publications/Files/Interim-guidance-on-the-use-of-
958 new-sea-level-rise-projections-August-2022.pdf
959 Mitchell, J. S., Mackay, K. A., Neil, H. L., Mackay, E. J., Pallentin, A., & Notman, P. (2012).
960 Undersea New Zealand, 1: 5,000,000. NIWA Chart, Miscellaneous Series, 92.
961 https://niwa.co.nz/our-science/oceans/bathymetry/further-information
962 Miyauchi, T., Ota, Y., & Hull, A. G. (1989). Holocene marine terraces and tectonic uplift in the
963 Waimarama coastal plain, eastern North Island, New Zealand. *New Zealand Journal of*
964 *Geology and Geophysics*, *32*(4), 437–442.
965 https://doi.org/10.1080/00288306.1989.10427551
966 Mountjoy, J. J., & Barnes, P. M. (2011). Active upper plate thrust faulting in regions of low plate
967 interface coupling, repeated slow slip events, and coastal uplift: Example from the
968 Hikurangi Margin, New Zealand. *Geochemistry, Geophysics, Geosystems*, *12*(1), n/a-n/a.
969 https://doi.org/10.1029/2010GC003326
970 Muis, S., Verlaan, M., Winsemius, H. C., Aerts, J. C. J. H., & Ward, P. J. (2016). A global
971 reanalysis of storm surges and extreme sea levels. *Nature Communications*, *7*(1), Article
972 1. https://doi.org/10.1038/ncomms11969

973 Naish, T., Levy, R. H., Hamling, I. J., Garner, G., Hreinsdóttir, S., Kopp, R. E., Golledge, N. R.,
974 Bell, R., Paulik, R., Lawrence, J., Denys, P. H., Gillies, T., Bengston, S., Clark, K., King,
975 D., Litchfield, N. J., Wallace, L., & Newnham, R. (2022). The significance of vertical
976 land movements at convergent plate boundaries in probabilistic sea-level projections for
977 AR6 scenarios: The New Zealand case. *Earth's Surface [Preprint]*.
978 https://doi.org/10.1002/essoar.10511878.1
979 Nikkhoo, M., & Walter, T. R. (2015). Triangular dislocation: An analytical, artefact-free
980 solution. *Geophysical Journal International*, *201*(2), 1119–1141.
981 https://doi.org/10.1093/gji/ggv035
982 Noda, H., & Lapusta, N. (2013). Stable creeping fault segments can become destructive as a
983 result of dynamic weakening. *Nature*, *493*(7433), 518–521.
984 https://doi.org/10.1038/nature11703
985 Okada, Y. (1985). Surface deformation due to shear and tensile faults in a half-space. *Bulletin of*
986 *the Seismological Society of America*, *75*(4), 1135–1154.
987 https://doi.org/10.1785/BSSA0750041135
988 Paquet, F., Proust, J.-N., Barnes, P. M., & Pettinga, J. R. (2009). Inner-forearc sequence
989 architecture in response to climatic and tectonic forcing since 150 ka: Hawke's Bay, New
990 Zealand. *Journal of Sedimentary Research*, *79*(3), 97–124.
991 https://doi.org/10.2110/jsr.2009.019
992 Paquet, F., Proust, J.-N., Barnes, P. M., & Pettinga, J. R. (2011). Controls on active forearc basin
993 stratigraphy and sediment fluxes: The Pleistocene of Hawke Bay, New Zealand.
994 *Geological Society of America Bulletin*, *123*(5–6), 1074–1096.
995 https://doi.org/10.1130/B30243.1

Perfettini, H., Avouac, J.-P., Tavera, H., Kositsky, A., Nocquet, J.-M., Bondoux, F., Chlieh, M., Sladen, A., Audin, L., Farber, D. L., & Soler, P. (2010). Seismic and aseismic slip on the Central Peru megathrust. *Nature*, *465*(7294), 78–81. https://doi.org/10.1038/nature09062

Peterson, C. D., Doyle, D. L., & Barnett, E. T. (2000). Coastal flooding and beach retreat from coseismic subsidence in the central Cascadia margin, USA. *Environmental and Engineering Geoscience*, *6*(3), 255–269. https://doi.org/10.2113/gseegeosci.6.3.255

Philibosian, B., & Meltzner, A. J. (2020). Segmentation and supercycles: A catalog of earthquake rupture patterns from the Sumatran Sunda Megathrust and other well-studied faults worldwide. Quaternary Science Reviews, 241, 106390. https://doi.org/10.1016/j.quascirev.2020.106390

Philibosian, B., Sieh, K., Avouac, J., Natawidjaja, D. H., Chiang, H., Wu, C., Shen, C., Daryono, M. R., Perfettini, H., Suwargadi, B. W., Lu, Y., & Wang, X. (2017). Earthquake supercycles on the Mentawai segment of the Sunda megathrust in the seventeenth century and earlier. *Journal of Geophysical Research: Solid Earth*, *122*(1), 642–676. https://doi.org/10.1002/2016JB013560

Pizer, C., Howarth, J., Clark, K., Howell, A., Delano, J., Hayward, B. W., & Litchfield, N. (2022). Variable polarity of coastal deformation confirms upper plate faulting as a partial driver of large magnitude earthquakes on the central Hikurangi subduction margin. Abstract T55A-06 presented at 2022 AGU Fall Meeting, 12-16 Dec.

Plafker, G. (1969). Tectonics of the March 27, 1964 Alaska Earthquake (U.S. Geological Survey Professional Paper No. 543–I; 74 p. https://pubs.usgs.gov/pp/0543i/

Power, W. (2013). Review of tsunami hazard in New Zealand (2013 update). *GNS Science Consultancy Report No. 2013*/131. https://www.civildefence.govt.nz/cdem-sector/cdem-

research-/mcdem-research-projects-and-resources/review-of-tsunami-hazard-in-new-zealand/

Savage, J. C. (1983). A dislocation model of strain accumulation and release at a subduction zone. *Journal of Geophysical Research: Solid Earth*, *88*(B6), 4984–4996. https://doi.org/10.1029/JB088iB06p04984

Seebeck, H., Van Dissen, R. J., Litchfield, N. J., Barnes, P. M., Nicol, A., Langridge, R. M., Barrell, D. J. A., Villamor, P., Ellis, S. M., & Rattenbury, M. S. (2022). *New Zealand Community Fault Model—Version 1.0*. https://doi.org/10.21420/GA7S-BS61

Sieh, K., Natawidjaja, D. H., Meltzner, A. J., Shen, C.-C., Cheng, H., Li, K.-S., Suwargadi, B. W., Galetzka, J., Philibosian, B., & Edwards, R. L. (2008). Earthquake Supercycles Inferred from Sea-Level Changes Recorded in the Corals of West Sumatra. *Science*, *322*(5908), 1674–1678. https://doi.org/10.1126/science.1163589

Sieh, K., Ward, S. N., Natawidjaja, D., and Suwargadi, B. W. (1999). Crustal deformation at the Sumatran Subduction Zone revealed by coral rings. *Geophysical Research Letters*, *26*(20), 3141–3144. https://doi.org/10.1029/1999GL005409

Stirling, M., Shaw, Bruce, Fitzgerald, M., and Ross, C. (2021). Selection and evaluation of magnitude–area scaling relations for update of the New Zealand National Seismic Hazard Model (p. 49). University of Otago.

Subarya, C., Chlieh, M., Prawirodirdjo, L., Avouac, J., Bock, Y., Sieh, K., Meltzner, A. J., Natawidjaja, D. H., and McCaffrey, R. (2006). Plate-boundary deformation associated with the great Sumatra–Andaman earthquake. *Nature*, 440(7080), Article 7080. https://doi.org/10.1038/nature04522

1041 Sweet, W. V., and Park, J. (2014). From the extreme to the mean: Acceleration and tipping
1042 points of coastal inundation from sea level rise. *Earth's Future*, *2*(12), 579–600.
1043 https://doi.org/10.1002/2014EF000272
1044 Tsang, L. L. H., Meltzner, A. J., Hill, E. M., Freymueller, J. T., and Sieh, K. (2015). A
1045 paleogeodetic record of variable interseismic rates and megathrust coupling at Simeulue
1046 Island, Sumatra. *Geophysical Research Letters*, *42*(24).
1047 https://doi.org/10.1002/2015GL066366
1048 Uchida, N., & Bürgmann, R. (2021). A Decade of Lessons Learned from the 2011 Tohoku-Oki
1049 Earthquake. *Reviews of Geophysics*, 59(2). https://doi.org/10.1029/2020RG000713
1050 Van Dissen, R. J., Seebeck, H., Wallace, L. M., Rollins, C., Gerstenberger, M. C., Howell, A., Di
1051 Caprio, C., & Williams, C. A. (2022). New Zealand National Seismic Hazard Model
1052 2022: Geologic and subduction interface deformation models. *GNZ Science Report*,
1053 *2022/31*. https://doi.org/10.21420/CEXY-AB93
1054 Wales, D. J., & Doye, J. P. K. (1997). Global optimization by basin-hopping and the lowest
1055 energy structures of Lennard-Jones clusters containing up to 110 atoms. *The Journal of*
1056 *Physical Chemistry A*, 101(28), 5111–5116. https://doi.org/10.1021/jp970984n
1057 Wallace, L. M. (2020). Slow Slip Events in New Zealand. *Annual Review of Earth and Planetary*
1058 *Sciences*, *48*(1), 175–203. https://doi.org/10.1146/annurev-earth-071719-055104
1059 Wallace, L. M., Beavan, J., Bannister, S., & Williams, C. (2012). Simultaneous long-term and
1060 short-term slow slip events at the Hikurangi subduction margin, New Zealand:
1061 Implications for processes that control slow slip event occurrence, duration, and
1062 migration. *Journal of Geophysical Research: Solid Earth*, *117*(B11), n/a-n/a.
1063 https://doi.org/10.1029/2012JB009489

1064 Wallace, L. M., Beavan, J., McCaffrey, R., & Darby, D. (2004). Subduction zone coupling and
1065 tectonic block rotations in the North Island, New Zealand. *Journal of Geophysical*
1066 *Research: Solid Earth*, *109*(B12). https://doi.org/10.1029/2004JB003241
1067 Wallace, L. M., Reyners, M., Cochran, U., Bannister, S., Barnes, P. M., Berryman, K., Downes,
1068 G., Eberhart-Phillips, D., Fagereng, A., Ellis, S., Nicol, A., McCaffrey, R., Beavan, R. J.,
1069 Henrys, S., Sutherland, R., Barker, D. H. N., Litchfield, N., Townend, J., Robinson, R.,
1070 … Power, W. (2009). Characterizing the seismogenic zone of a major plate boundary
1071 subduction thrust: Hikurangi Margin, New Zealand. *Geochemistry, Geophysics,*
1072 *Geosystems*, *10*(10), n/a-n/a. https://doi.org/10.1029/2009GC002610
1073 Wang, K., & Bilek, Susan L. (2014). Invited review paper: Fault creep caused by subduction of
1074 rough seafloor relief. *Tectonophysics*, 610, 1–24.
1075 https://doi.org/10.1016/j.tecto.2013.11.024
1076 Wang, K., Hu, Y., & He, J. (2012). Deformation cycles of subduction earthquakes in a
1077 viscoelastic Earth. *Nature*, 484(7394), 327–332. https://doi.org/10.1038/nature11032
1078 Wang, L., Hainzl, S., & Mai, P. M. (2015). Quantifying slip balance in the earthquake cycle:
1079 Coseismic slip model constrained by interseismic coupling. *Journal of Geophysical*
1080 *Research: Solid Earth*, *120*(12), 8383–8403. https://doi.org/10.1002/2015JB011987
1081 Wesson, R. L., Melnick, D., Cisternas, M., Moreno, M., & Ely, L. L. (2015). Vertical
1082 deformation through a complete seismic cycle at Isla Santa María, Chile. *Nature*
1083 *Geoscience*, *8*(7), 547–551. https://doi.org/10.1038/ngeo2468
1084 Williams, C. A., Eberhart-Phillips, D., Bannister, S., Barker, D. H. N., Henrys, S., Reyners, M.,
1085 & Sutherland, R. (2013). Revised interface geometry for the Hikurangi Subduction Zone,

New Zealand. *Seismological Research Letters*, *84*(6), 1066–1073. https://doi.org/10.1785/0220130035

Witter, R., Briggs, R., Dura, T., Engelhart, S., & Nelson, A. (2022). Seismic sources in the Aleutian cradle of tsunamis. *Eos*, *103*. https://doi.org/10.1029/2022EO220464

Witter, R., Briggs, R., Engelhart, S. E., Gelfenbaum, G., Koehler, R. D., Nelson, A., Selle, S. L., Corbett, R., & Wallace, K. (2019). Evidence for frequent, large tsunamis spanning locked and creeping parts of the Aleutian megathrust. *GSA Bulletin*, *131*(5–6), 707–729. https://doi.org/10.1130/B32031.1

Witter, R., Briggs, R. W., Engelhart, S. E., Gelfenbaum, G., Koehler, R. D., & Barnhart, W. D. (2014). Little late Holocene strain accumulation and release on the Aleutian megathrust below the Shumagin Islands, Alaska. *Geophysical Research Letters*, *41*(7), 2359–2367. https://doi.org/10.1002/2014GL059393

Woods, K. (2022). *Investigation of Hikurangi subduction zone slow slip events using onshore and offshore geodetic data* [Open Access Te Herenga Waka-Victoria University of Wellington]. https://doi.org/10.26686/wgtn.21300411

Figure 1: setting.

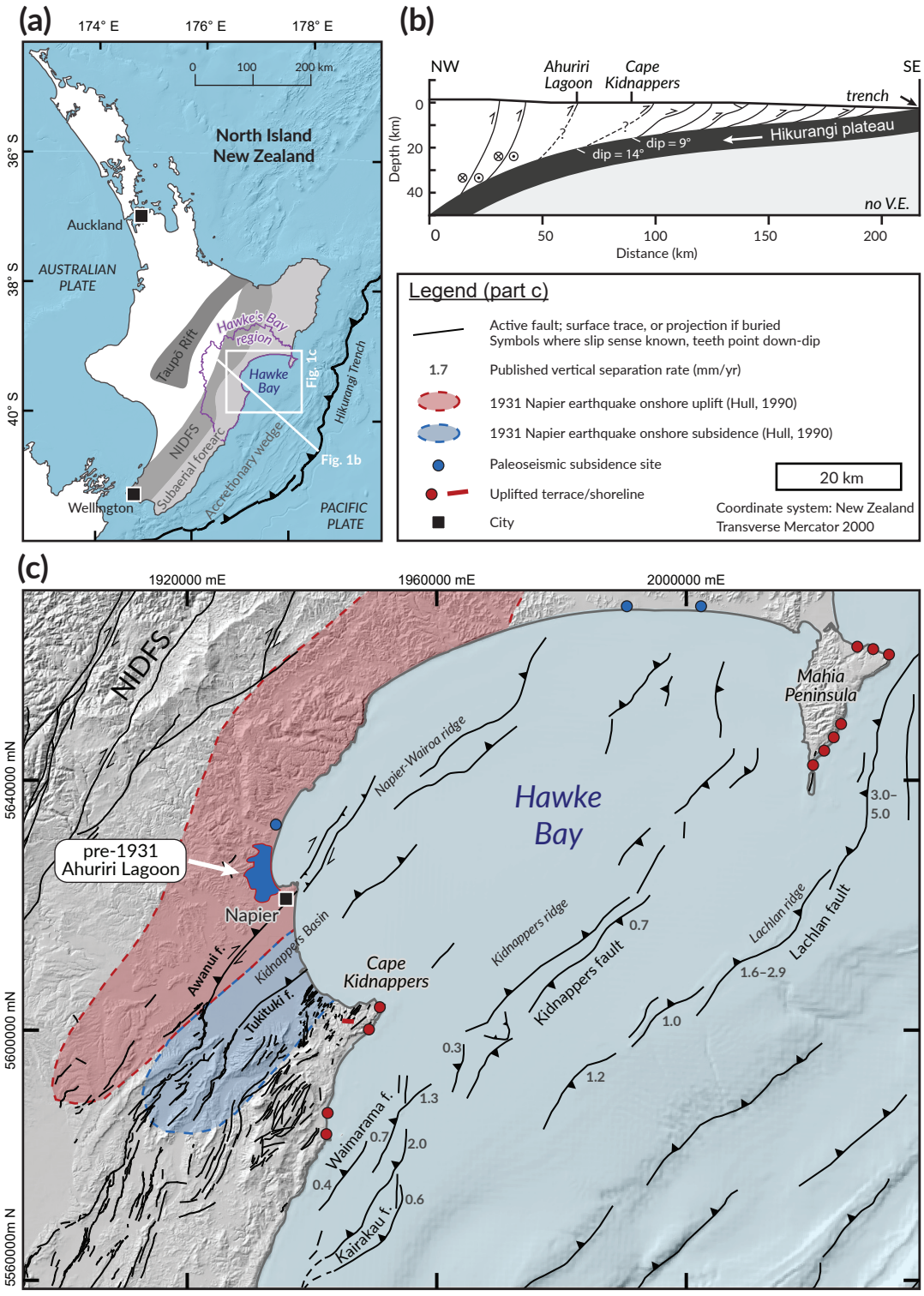
(a)
174° E
176° E
178° E
36° S
38° S
40° S
0
100
200 km
North Island
New Zealand
Auckland
AUSTRALIAN PLATE
Taupō Rift
Hawke's Bay region
Hawke Bay
Fig. 1c
Hikurangi Trench
NIDFS
Subaerial forearc
Accretionary wedge
Fig. 1b
Wellington
PACIFIC PLATE
(b)
NW
Ahuriri Lagoon
Cape Kidnappers
SE
trench
Depth (km)
0
20
40
dip = 14°
dip = 9°
Hikurangi plateau
no V.E.
0
50
100
150
200
Distance (km)
Legend (part c)
Active fault; surface trace, or projection if buried
Symbols where slip sense known, teeth point down-dip
1.7
Published vertical separation rate (mm/yr)
1931 Napier earthquake onshore uplift (Hull, 1990)
1931 Napier earthquake onshore subsidence (Hull, 1990)
Paleoseismic subsidence site
Uplifted terrace/shoreline
City
20 km
Coordinate system: New Zealand Transverse Mercator 2000
(c)
1920000 mE
1960000 mE
2000000 mE
5640000 mN
5600000 mN
5560000m N
NIDFS
Napier-Wairoa ridge
Hawke Bay
Mahia Peninsula
3.0–5.0
pre-1931 Ahuriri Lagoon
Napier
Awanui f.
Kidnappers Basin
Tukituki f.
Cape Kidnappers
Kidnappers ridge
0.7
Kidnappers fault
Lachlan ridge
Lachlan fault
1.6–2.9
1.0
0.3
1.2
1.3
Waimarama f.
0.7
2.0
0.4
0.6
Kairakau f.

Figure 2: displacement schematic.

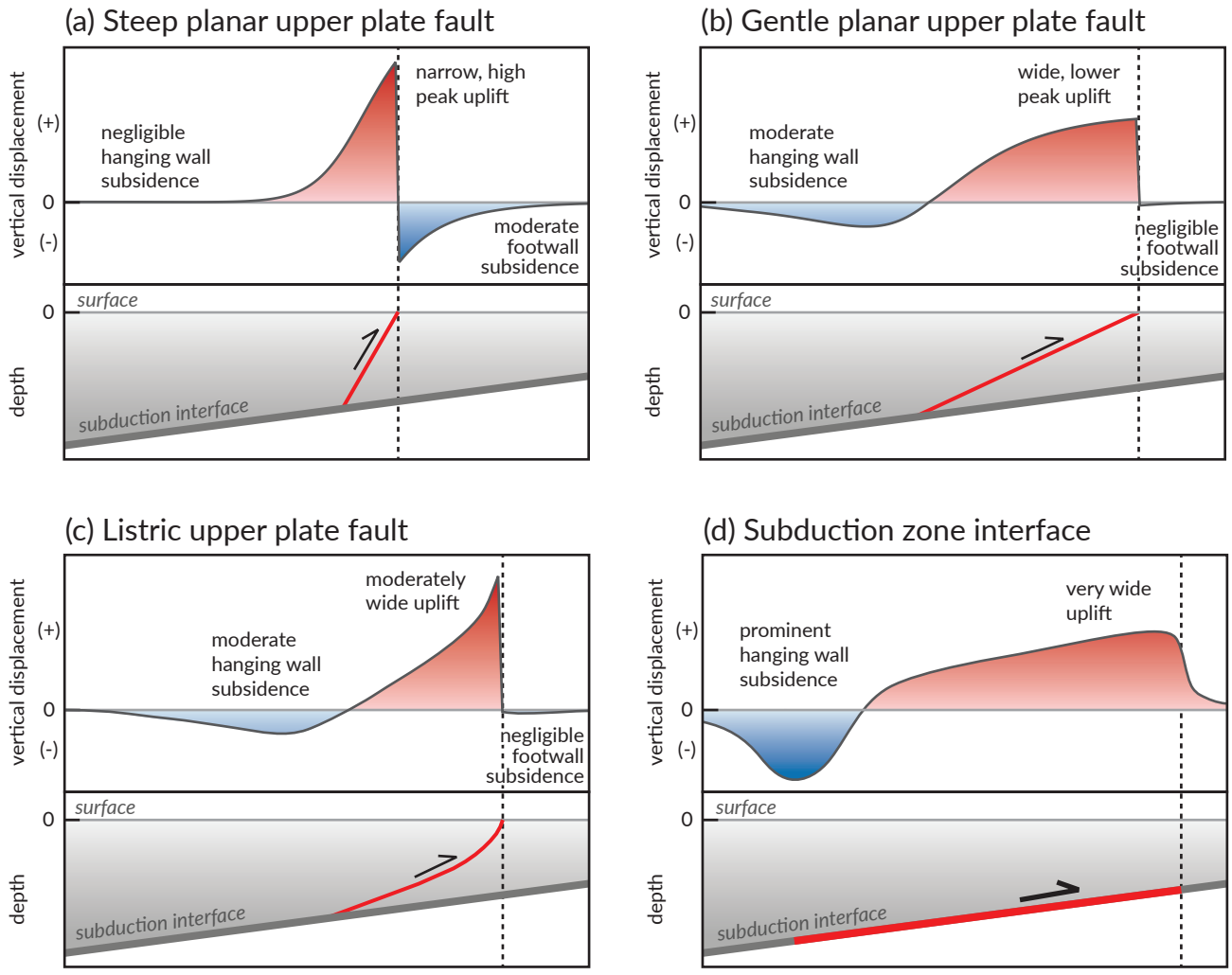

schematic; not to scale

Figure 3: paleoseismic sites.

(a)

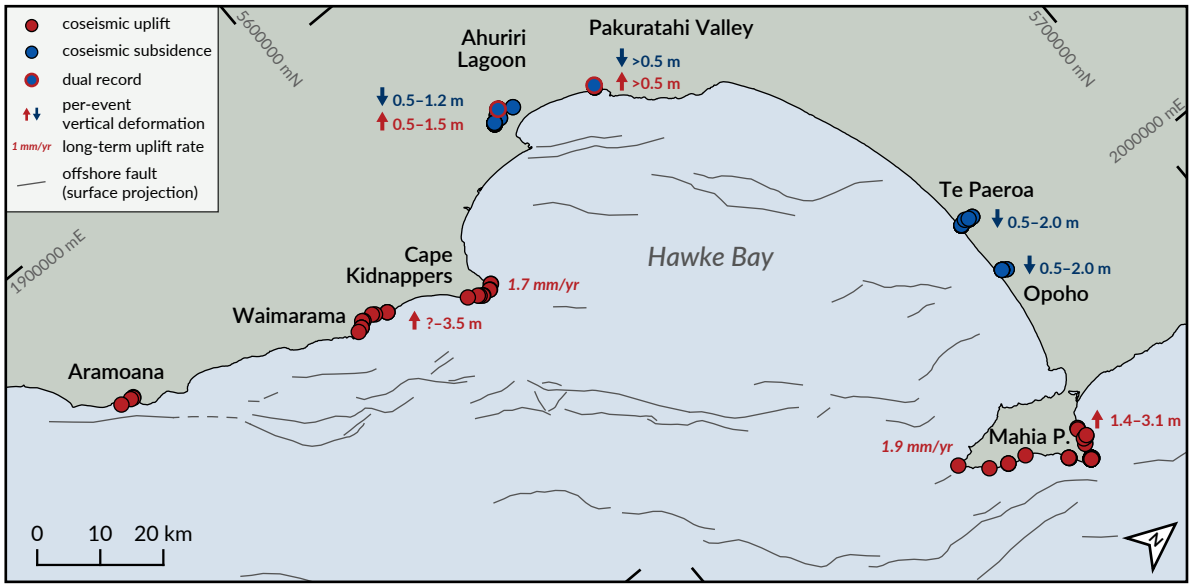
coseismic uplift
coseismic subsidence
dual record
per-event vertical deformation
1 mm/yr
long-term uplift rate
offshore fault (surface projection)
5600000 mN
5700000 mN
1900000 mE
2000000 mE
Ahuriri Lagoon
0.5–1.2 m
0.5–1.5 m
Pakuratahi Valley
>0.5 m
>0.5 m
Te Paeroa
0.5–2.0 m
0.5–2.0 m
Opoho
Hawke Bay
Cape Kidnappers
1.7 mm/yr
Waimarama
?–3.5 m
Aramoana
1.4–3.1 m
1.9 mm/yr
Mahia P.
0 10 20 km
N

(b)

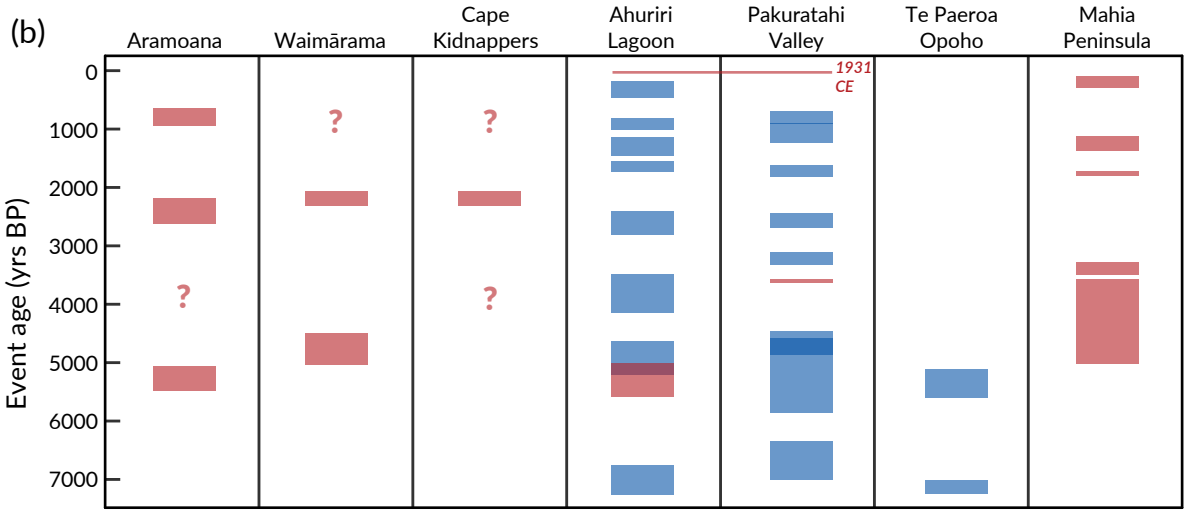
Aramoana
Waimārama
Cape Kidnappers
Ahuriri Lagoon
Pakuratahi Valley
Te Paeroa Opoho
Mahia Peninsula
1931 CE
Event age (yrs BP)
0
1000
2000
3000
4000
5000
6000
7000
?

Figure 4: UPF results.

(a) Listric upper plate fault, rake = 90

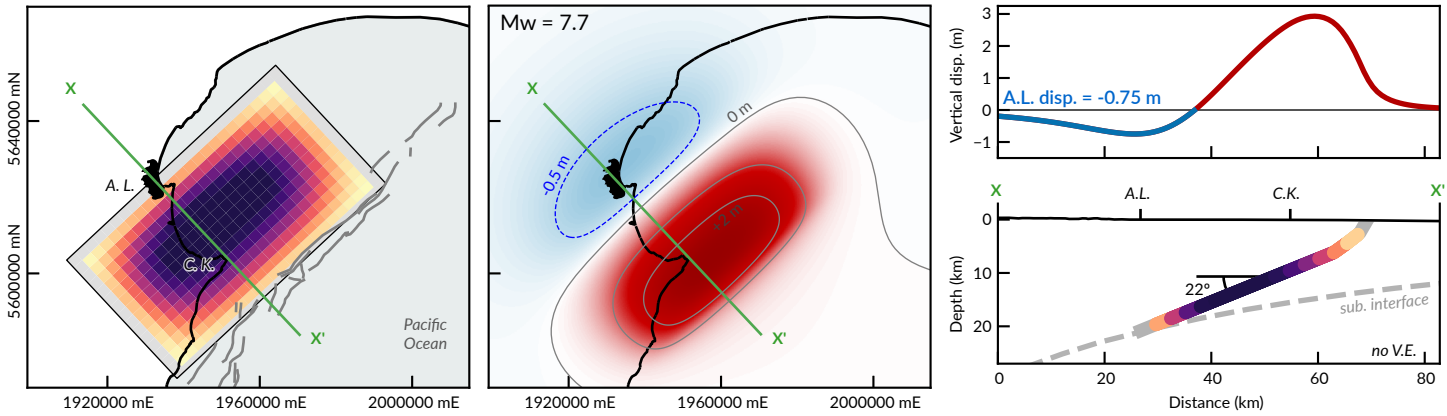

(b) Listric upper plate fault, rake = 135

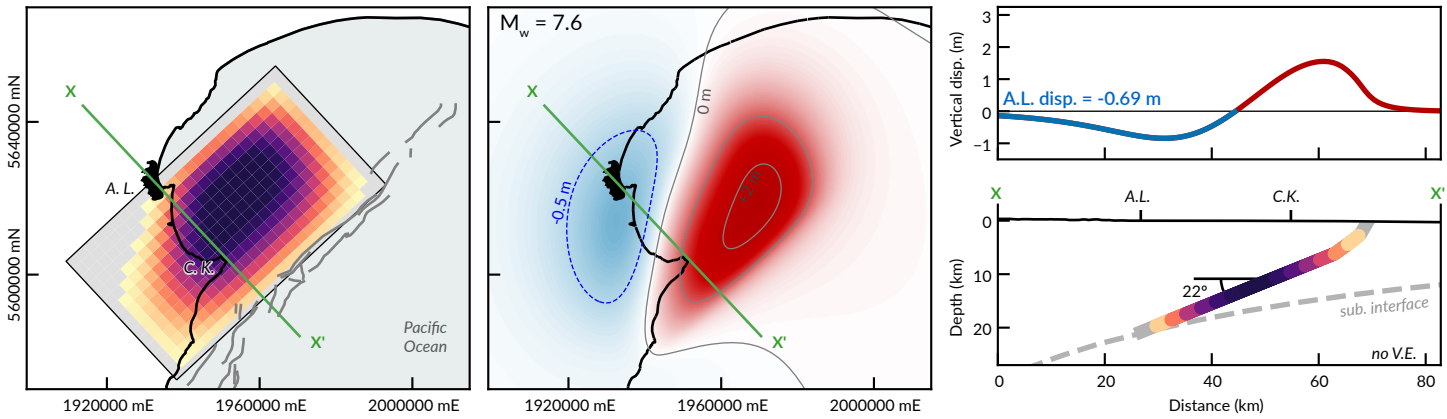

(c) Planar fault + subduction interface, rake = 135

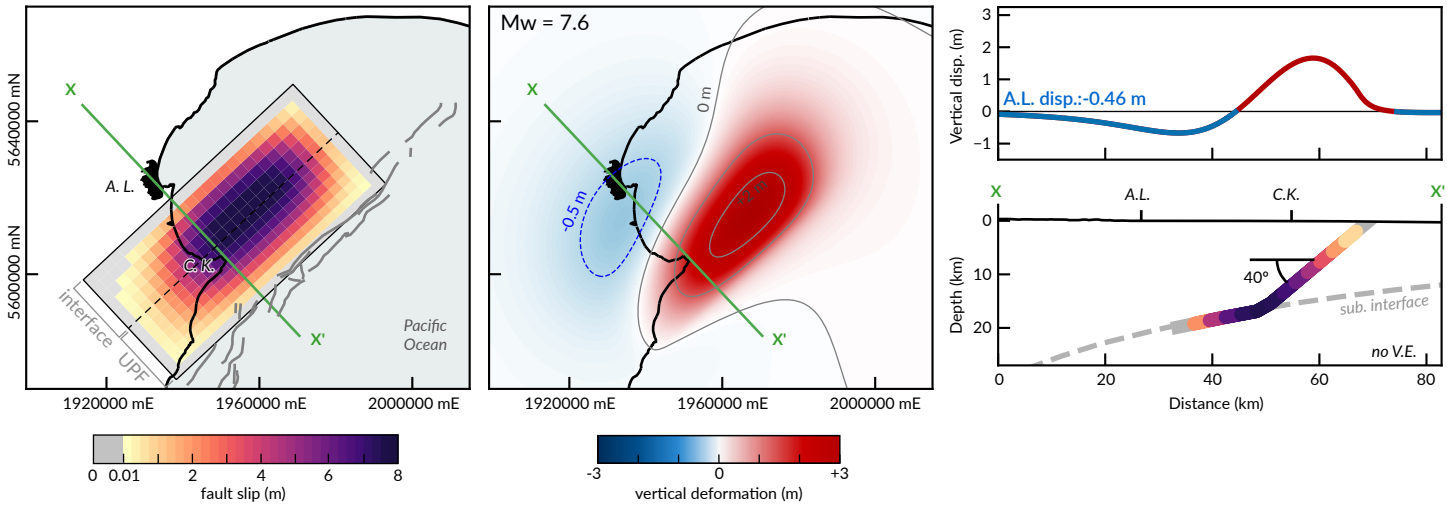

Figure 5: SZ results.

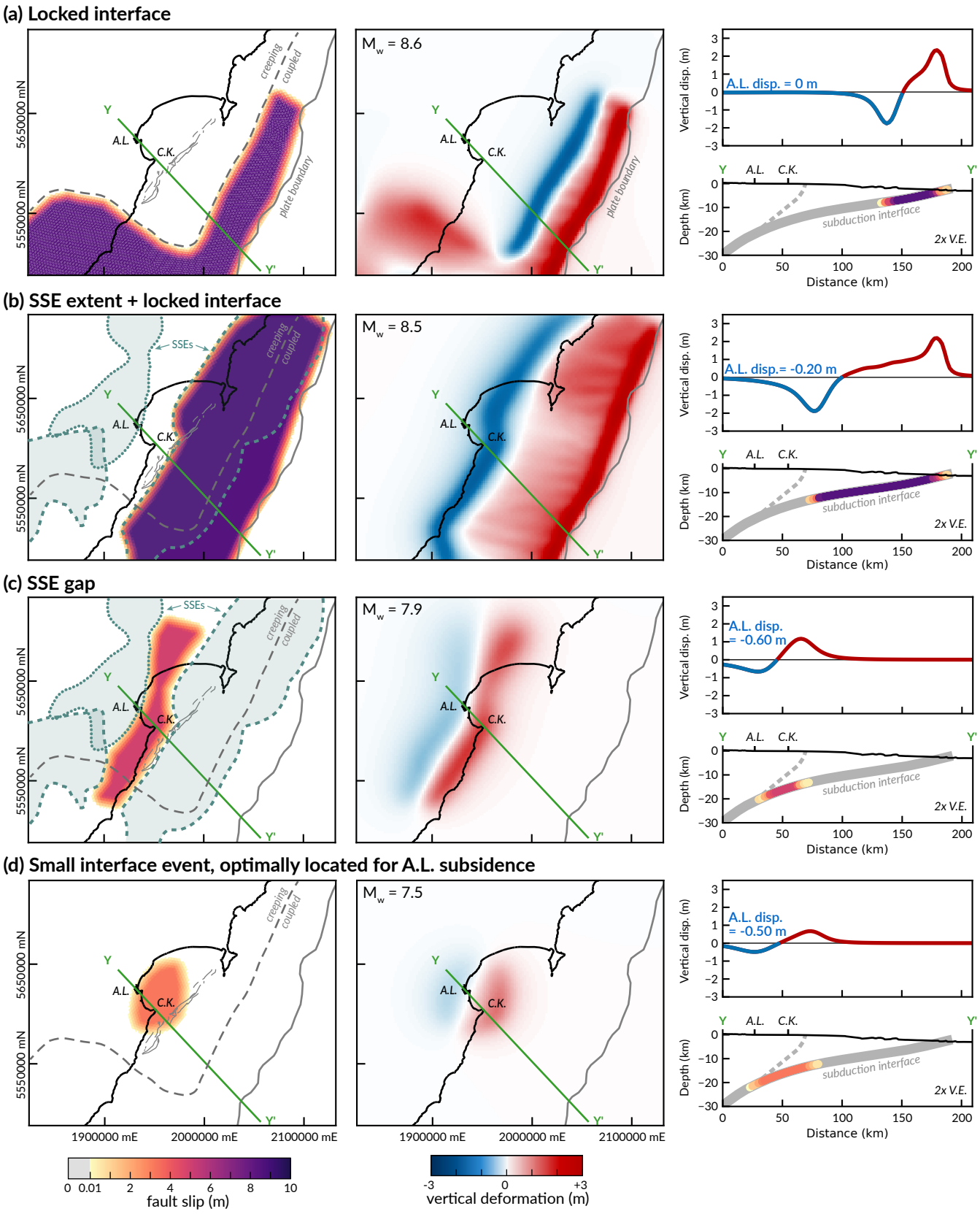
(a) Locked interface
(b) SSE extent + locked interface
(c) SSE gap
(d) Small interface event, optimally located for A.L. subsidence
creeping
coupled
plate boundary
SSEs
A.L.
C.K.
Y
Y'
5650000 mN
5550000 mN
M_w = 8.6
M_w = 8.5
M_w = 7.9
M_w = 7.5
A.L. disp. = 0 m
A.L. disp.= -0.20 m
A.L. disp. = -0.60 m
A.L. disp. = -0.50 m
Vertical disp. (m)
Depth (km)
subduction interface
2x V.E.
Distance (km)
1900000 mE
2000000 mE
2100000 mE
0 0.01 2 4 6 8 10
fault slip (m)
-3 0 +3
vertical deformation (m)